

ISSN 1883 - 0315



TOHOKU
UNIVERSITY

IMR **KINKEN** Research Highlights 2019

Institute for Materials Research, Tohoku University



Research

KINKEN

Research Highlights

2019



Institute for Materials Research, Tohoku University

KINKEN Research Highlights 2019

Contents

Preface	4
----------------------	---

Research Highlights

1. Infrastructural Materials

Microstructure Design of Structural Metallic Materials Research Laboratory.....	8
Environmentally Robust Materials Research Laboratory.....	9
Advanced Crystal Engineering Laboratory	10
Deformation Processing Research Laboratory	11
Analytical Science Research Laboratory	12
Creation of Life Innovation Materials for Interdisciplinary and International Researcher Development.....	13
Professional development Consortium for Computational Materials Scientists (PCoMS)	14

2. Energy-Related Materials

Crystal Physics Research Laboratory	16
Materials Design by Computer Simulation Research Laboratory.....	17
Nuclear Materials Engineering Research Laboratory	18
Chemical Physics of Non-Crystalline Materials Research Laboratory	19
Structure-Controlled Functional Materials Research Laboratory	20
Non-Equilibrium Materials Research Laboratory.....	21
Magnetic Materials Research Laboratory	22
Hydrogen Functional Materials Research Laboratory	23

3. Electronic Materials

Theory of Solid State Physics Research Laboratory	26
Magnetism Research Laboratory	27
Surface and Interface Research Laboratory	28
Low Temperature Physics Research Laboratory	29
Low Temperature Condensed State Physics Research Laboratory	30
Quantum Beam Materials Physics Research Laboratory	31
Quantum Functional Materials Physics Research Laboratory	32
Irradiation Effects in Nuclear and Their Related Materials Research Laboratory	33
Physics of Electronic Materials Research Laboratory	34
Solid-State Metal-Complex Chemistry Research Laboratory	35
Crystal Chemistry Research Laboratory	36
Actinide Materials Science Research Laboratory	37
Materials Science of Non-Stoichiometric Compounds Research Laboratory	38

Research Centers

International Research Center for Nuclear Materials Science	40
Cooperative Research and Development Center for Advanced Materials	42
High Field Laboratory for Superconducting Materials	43
Trans-Regional Corporation Center for Industrial Materials Research	44
Collaborative Research Center on Energy Materials	45
Center for Computational Materials Science	46
International Collaboration Center	47
Center of Neutron Science for Advanced Materials	48
Laboratory of Low Temperature Materials Science	49
Laboratory of Alpha-Ray Emitters	50
Analytical Research Core for Advanced Materials	51

Author Index	52
---------------------------	----

Keyword Index	53
----------------------------	----



Preface

Dear Colleagues,

We are pleased to present *KINKEN* Research Highlights 2019, which is the annual report that includes a collection of research outputs of the past year from the Institute for Materials Research (IMR), Tohoku University. *KINKEN* is the abbreviation for “Kinzoku Zairyo Kenkyujo,” the Japanese name for IMR, which is well known in the materials science community.

IMR celebrated its centenary in 2016. Professor Kotaro Honda established the IMR at the Tohoku Imperial University in 1916 as the 2nd Division of the Provisional Institute of Physical and Chemical Research. At that time the primary research focus was steel. Thereafter, the research domains gradually broadened to include various types of alloys and metals. The name was changed into the Research Institute for Iron, Steel and Other Metals (RIISOM) in 1922. Subsequently, the institute developed into a global center for fundamental and applied research covering all types of materials, including nonmetals. In 1987 the institute was reorganized into a national collaborative research institute affiliated with Tohoku University, and consequently renamed to the present Institute for Materials Research (IMR).

IMR has greatly contributed to the advancement of materials science and engineering. The invention of KS steel in 1916, the strongest permanent magnet at that time, was the first great achievement. In subsequent years, many different types of practically useable materials have successfully been developed, including new KS steel, Sendust alloy, SiC fibers, various intermetallic compounds, and more recently, amorphous alloys. In addition, considerable effort was dedicated to basic research for materials development, which paved the way for pioneering research in magnetism, superconductivity,



Director Prof. Koki Takanashi



optical properties, and microstructure analyses of materials. Recently, IMR has created a wide array of new materials, including high-performance, high-quality, and multifunctional materials such as bulk metallic glasses, nanostructured materials, nanocomposites, ceramics, crystals, oxides, nitrides, hydrides, complexes, organic materials, etc., which are useful for electronic, optical, magnetic, spintronic, biological, energetic, and infrastructural applications.

In the 21st Century, we face worldwide environmental problems such as global warming and the depletion of resources and energy. There is an increasing need to preserve the environment and work towards achieving sustainable societies. IMR upholds these themes with the objective of “contributing to the well being of the human race and the development of civilization through the creation of new materials that are truly useful to society”.

We hope that the KINKEN Research Highlights will enable you to better understand our recent research activities and will aid the promotion of worldwide collaboration with IMR. We ask for your continued support and welcome any suggestions.

Infrastructural Materials

IMR KINKEN Research Highlights 2019



Microstructure of Reverted Austenite in Fe-0.3N Martensite

The reverse transformation behavior during inter-critical annealing was studied in Fe-0.3mass%N binary alloy. Two morphologies of acicular and globular austenite are formed during the reversion process. The globular austenite has almost the same orientation as one of adjacent prior austenite grains and grows into the martensite with a larger deviation angle from the Kurdjumov–Sachs orientation relationship (K-S OR). In contrast, the acicular austenite holds a near K-S OR with its surrounding martensite matrix. A large amount of retained austenite was obtained through simple inter-critical annealing owing to an enrichment of nitrogen in the reverted austenite.

Nitrogen, an interstitial element frequently used in steel other than carbon, thermodynamically stabilizes austenite (γ) and shows a similar tendency to that of carbon in terms of the change in M_s temperature or lattice parameter change [1, 2]. In contrast, nitrogen has larger solubility limits in ferrite (α) or γ phases with respect to ferrous nitride than in the case of carbon with respect to cementite, leading to a higher eutectoid composition and a lower eutectoid temperature. It is therefore possible to decrease the annealing temperature in $\alpha + \gamma$ two-phase region, and to enrich more nitrogen into γ , thereby implying that more retained austenite can be obtained.

In this study, Fe-0.3mass%N martensite was prepared using the nitriding and quenching (N-Q) process [3]. A sample was then heated to 650–750 °C within the $\alpha + \gamma$ two-phase region and inter-critically annealed for 3–3,600 s. The microstructures of the heat-treated samples were observed using FE-SEM, and the volume fractions of the constituent phases were determined through point counting and XRD.

Figure 1 shows the microstructure evolution during inter-critical annealing at 650 °C and 750 °C. Two types of reverted γ were observed, namely, globular austenite (γ_G) nucleated at the prior γ grain boundary, and acicular austenite (γ_A) nucleated at both the lath and block boundaries of martensite. This reverse transformation behavior is extremely similar to that of carbon-containing alloys [4].

Figure 2 shows the reverse transformation kinetics curves at 650 and 750 °C. At each temperature, the volume fraction of the reverted γ increased with an increase in the holding time and eventually reached equilibrium. The γ retained was obtained at each temperature, the maximum value of which was approximately 6% at 750 °C, and approximately 10% at 650 °C. It was confirmed that simple inter-critical annealing can achieve a large amount of retained austenite in nitrogen-contained steel.

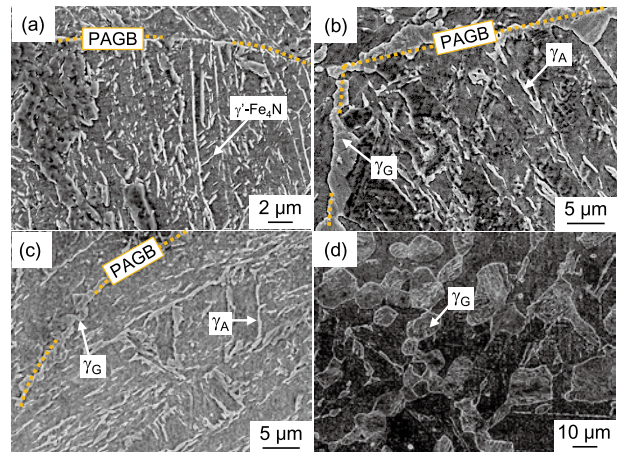


Fig. 1 SEM images of Fe-0.3N alloy annealed at (a) 650 °C for 3 s, (b) 650 °C for 3,600 s, (c) 750 °C for 3 s, and (d) 750 °C for 3,600 s.

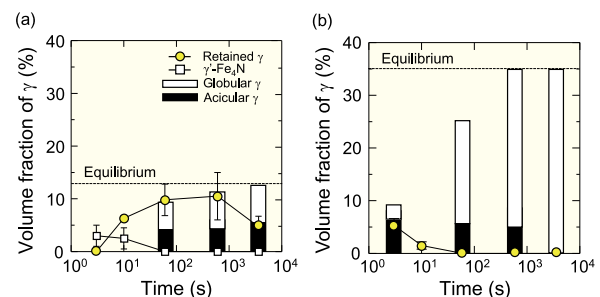


Fig. 2 Reverse transformation kinetics curves of Fe-0.3N alloy annealed at (a) 650 °C and (b) 750 °C.

References

- [1] L. Chen and E. J. Mittemeijer, *Scripta Metall. Mater.* **24**, 509 (1990).
- [2] T. Bell and J. Iron Steel Inst. **206**, 1017 (1968).
- [3] J. Takeuchi, T. Iguchi, and T. Ishihara, *J. Jpn. Soc. Heat Treatment* **21**, 26 (1981).
- [4] X.-G. Zhang, G. Miyamoto, Y. Toji, S. Nambu, T. Koseki, and T. Furuhashi, *Acta Mater.* **144**, 601 (2018).

Keywords: steel, phase transformation, microstructure

Mitsutaka Sato (Microstructure Design of Structural Metallic Materials Research Laboratory)

E-mail: m-sato@imr.tohoku.ac.jp

URL: <http://www.st-mat.imr.tohoku.ac.jp>

Hydrogen Embrittlement Property of a High Strength TRIP-Aided Bainitic Ferrite Steel

Our investigation based on a tensile test of hydrogen-charged Transformation induced plasticity (TRIP) aided bainite ferrite steel showed a tensile strength of 1.2 GPa at various strain rates, and microscopic observations indicated that hydrogen-induced crack initiation from the martensitic transformation of the retained austenite, and subsequent crack propagation under the existence of hydrogen, are key factors.

Transformation induced plasticity (TRIP) aided bainite ferrite (TBF) steel with a bainitic ferrite matrix exhibits excellent formability and impact and fatigue properties, and thus the use of such steel is expected for automotive frame parts. However, owing to a high strength, hydrogen embrittlement (HE) is an unavoidable subject, as is the use of twinning induced plasticity (TWIP) steel [1]. Although it has been reported that the HE resistance of TRIP steel evaluated through a tensile test is affected by the strain rate, the effect of the strain rate on the HE of TBF steel has yet to be clarified. Our present study aims at clarifying the role of the strain rate on the HE behavior and an understanding of the mechanism of the HE of TBF steel [2].

Figure 1 shows the change in total elongation (TEI) and the time to fracture of hydrogen-charged TBF steel with a tensile strength of 1.2 GPa as a function of the strain rate. Clearly, TEI decreases as the strain rate decreases; *i.e.*, the susceptibility of steel to HE was enhanced. Because the time to fracture monotonically increases with a decrease in the strain rate, the apparent susceptibility to HE is presumably influenced by hydrogen diffusion.

Observations of the fracture surface and cross section revealed that facets (Fig. 2) were formed in hydrogen-charged steel owing to the martensitic transformation of the retained austenite and to the supersaturation of hydrogen in the newly formed martensite caused by a significant loss of the hydrogen solubility.

The facet formation marks the beginning of a fracture, and an accumulation of diffusible hydrogen from the matrix and the martensite transformed from the retained austenite within the vicinity of the tips of the initiated facets is likely necessary for crack propagation, and is thus considered to be the reason for the strain rate dependence of the total elongation.

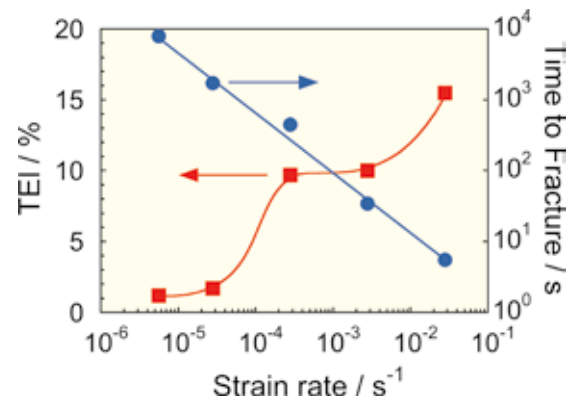


Fig. 1 Effects of strain rate on the total elongation and time to fracture of a TBF steel.

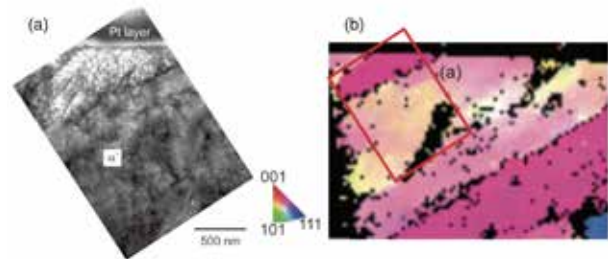


Fig. 2 (a) Transmission electron micrograph and (b) inverse pole figure map around a facet formed in hydrogen-precharged TBF steel tested at $5.56 \times 10^{-6} \text{ s}^{-1}$.

References

- [1] I. B. Tuğluca, M. Koyama, B. Balb, D. Canadinc, E. Akiyama, and K. Tsuzaki: *Mater. Sci. Eng. A* **717**, 78 (2018).
- [2] T. Hojo, R. Kikuchi, H. Waki, F. Nishimura, Y. Ukai, and E. Akiyama: *ISIJ Int.* **58**, 751 (2018).

Growth and Scintillation Properties of Two-Inch-Diameter Eu:SrI₂ Single Crystals

Eu-doped SrI₂ (Eu:SrI₂) has been recognized as a high-performance scintillator with a high light yield and high energy resolution. In this study, we successfully grew Eu:SrI₂ single crystals 2-inch in diameter and 4-inch in length. The light output of the 2-inch diameter Eu:SrI₂ was estimated to be 70,000 photons/MeV, and the calculated energy resolution was 3.4% (662 keV, FWHM) at room temperature.

Eu-doped SrI₂ (Eu:SrI₂) single crystals have been studied intensively owing to their possible applications in radiation detectors. A growth system simply representing a seeded Bridgman technique was recently developed, and the growth of Eu-doped SrI₂ crystals of 1 inch in diameter was established [1]. However, the crystals reported in Ref. [1] are not crack-free, and their dimensions are insufficient for many practical applications. Therefore, the purpose of the current study was to develop a crystal growth process suitable for the fabrication of relatively large (more than 2 inches in diameter) and macro-defect-free crystals [2, 3].

The Eu:SrI₂ single crystals were grown from the melt of a (Sr_{0.98}Eu_{0.02})I₂ composition using carbon crucibles. The 2-inch diameter macro-defect-free Eu:SrI₂ crystals were grown using a vertical Bridgman method with a crystal growth apparatus that was originally designed for the micro-pulling-down crystal growth process.

The number of bubbles captured by the crystals was considerably reduced after preliminary vacuum degassing. The decrease in the temperature of the melt during the initial stage of growth with the corresponding elimination of the seed over-melting resulted in the formation of macro-defect-free Eu:SrI₂ crystals. An additional treatment of the interior of the crucible results in reduced wetting between the SrI₂ melt and the crucible approaching the Liquinert process (Fig. 1). A cut and packaged Eu:SrI₂ specimen (2 inches in diameter and length) demonstrated a light output exceeding 70,000 photons/MeV and an energy resolution of 3.4% (662 keV, FWHM).

After an evaluation of single crystals, we developed Eu:SrI₂ array detectors. The photographs of the developed Eu:SrI₂ arrays are shown in Fig. 2. Fig. 2(a) shows a 4 x 4 matrix and a 3 x 3 x 3 mm³ pixel array, and the right side of Fig. 2(b) shows a 9 x 9 matrix and a 1 x 1 x 1 mm³ pixel array. We obtained the best energy resolution of 4.1% (FWHM) at a gamma-ray of 662 keV.

References

- [1] Y. Yokota, K. Nishimoto, K. Kurosawa, D. Totsuka, and A. Yoshikawa, *J. Cryst. Growth* **375**, 49 (2013).
 [2] A. Yoshikawa, Y. Shoji, Y. Yokota, S. Kurosawa, S. Hayasaka, V. I. Chani, T. Ito, K. Kamada, Y. Ohashi, V. Kochurikhin, and A. Yoshikawa,

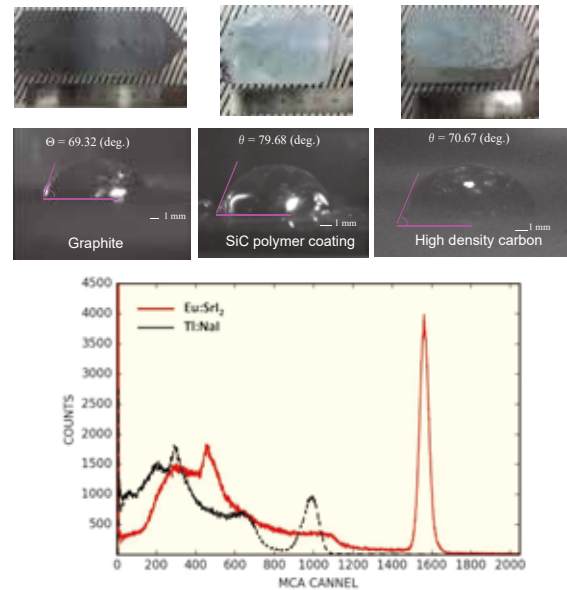


Fig. 1 Top, SrI₂ crystals produced from different crucibles; middle, their corresponding wetting angles; and bottom, the pulse height spectra of Eu:SrI₂. Specimen and TI doped NaI.

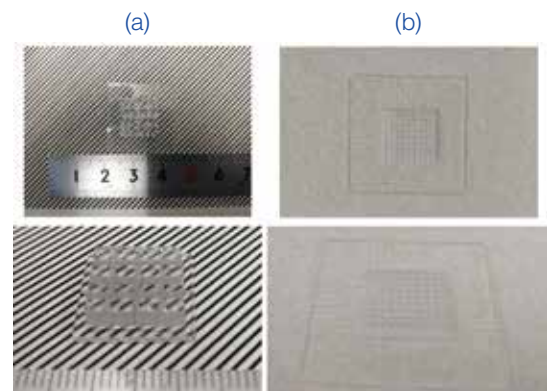


Fig. 2 Photographs of developed Eu:SrI₂ arrays. (a), 3 x 3 x 3 mm³ and 4 x 4 matrix; (b), 1 x 1 x 1 mm³ and 9 x 9 matrix.

J. Cryst. Growth **452**, 73 (2016).

- [3] Y. Shoji, S. Kurosawa, Y. Yokota, S. Hayasaka, K. Kamada, M. Yoshino, A. Yamaji, V. Chani, Y. Ohashi, S. Sakuragi, and A. Yoshikawa, *Cryst. Growth Des.* **18**, 3747 (2018).

Keywords: scintillator, crystal growth

Akira Yoshikawa (Advanced Crystal Engineering Laboratory)

E-mail: yoshikawa@imr.tohoku.ac.jp

URL: <http://yoshikawa-lab.imr.tohoku.ac.jp/index.html>

Electron Beam Melting of Boron-Modified Ti-6Al-2Sn-4Zr-2Mo-0.1Si Alloy with Superior Tensile Strength and Oxidation Resistance

We succeeded in fabricating Ti-6Al-2Sn-4Zr-2Mo-0.1Si-1B alloy with superior tensile strength and oxidation resistance by applying an electron beam melting (EBM) additive manufacturing process. Owing to the rapid solidification process during EBM, much finer TiB precipitates with a nanometer width are obtained in an EBM built alloy as compared with a wrought alloy. These refined TiB precipitates contribute to an enhanced strength and greater oxidation resistance.

Electron beam melting (EBM) is an innovative additive manufacturing process whereby various parts are created layer by layer directly from a computer-aided design file. This has promising advantages such as a design freedom and high efficiency, and can easily be used to fabricate defect-free components with complex shapes and a low residual stress. Titanium and its alloys are of significant interest regarding EBM because Ti alloys combine broad industry applications with high machining costs and long lead times in conventional processing.

In the aerospace industry, lightweight engines are a key to improving the fuel efficiency. Lighter heat-resistant Ti-based alloys are expected to be developed to replace heavy Ni-based alloys used for high-pressure compressor blades where both a high strength and significant oxidation resistance at high temperatures are required.

Ti-6Al-2Sn-4Zr-2Mo-0.1Si alloy, often referred to as Ti-6242S, has been chosen as a heat-resistant Ti alloy. It was reported that TiB precipitates can improve the strength of Ti-based alloys owing to their good mechanical properties, high thermal stability, and a similar thermal expansion as that of a Ti matrix [1]. However, coarse-sized TiB precipitates formed through conventional casting or forging have a limited contribution to strength.

Much finer and more uniformly dispersed TiB precipitates are obtained in EBM built alloy as compared with conventional wrought alloy, as shown in Fig. 1. This is mainly ascribed to the rapid solidification process during EBM. These refined TiB precipitates can act more effectively as obstacles of dislocation motion. Consequently, the tensile strength of EBM specimens is higher than that of the wrought specimens at elevated temperatures of up to 873 K. The tensile strength of an EBM specimen at 873 K was approximately 1.4-times that of a wrought specimen, as shown in Fig. 2.

In addition, the oxidation resistance was also

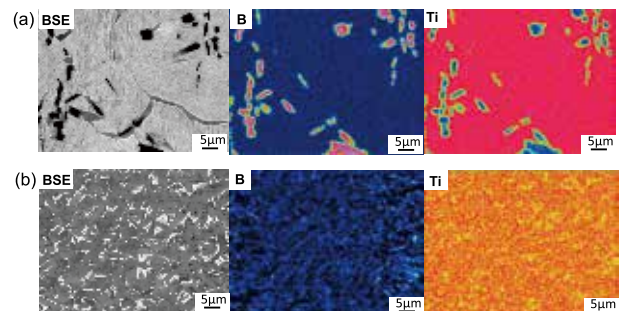


Fig. 1 SEM-BSE images and EPMA elemental mappings of B and Ti of (a) wrought and (b) EBM specimens [2].

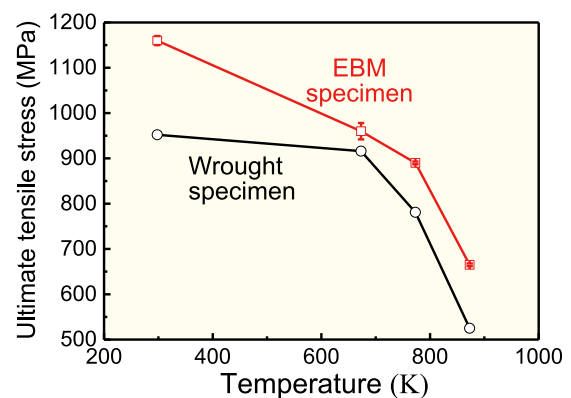


Fig. 2 Temperature dependence of ultimate tensile stress in wrought and EBM specimens [2].

significantly improved in EBM built alloy as compared with a conventional wrought alloy.

This improvement is mainly ascribed to the formation of dense oxidation layers caused by the homogenous dispersion of fine TiB precipitates, which prevents further oxidation in EBM built alloy.

References

- [1] X. Guo, L. Wang, M. Wang, J. Qin, D. Zhang, and W. Lu, *Acta Mater.* **60**, 2656 (2012).
- [2] T. Fujieda, Y. Cui, K. Aoyagi, Y. Koizumi, and A. Chiba, *Materialia*. **4**, 367 (2018).

Comparison of Coherent Forward Scattering and Atomic Absorption Profiles of Ar 842.5-nm Line in Pulsed Radio Frequency Glow-Discharge Plasma

A comparison of the coherent forward scattering (CFS) and atomic absorption (AA) of an Ar I 842.5-nm line was conducted using pulsed radio-frequency (RF) glow discharge (GD) plasma. The locations of the highest and second-highest number densities of the excited argon atoms in the lower state of an Ar I 842.5-nm transition could be determined.

The coherent forward scattering (CFS) technique is based on two crossed polarizers, a polarizer and an analyzer, which block the probe light when no atomic interactions occur. Because of the anisotropy of resonant analyte atoms, which is induced by the external magnetic field applied, the state of light polarization is changed when passing through the atomic vapor between the polarizer and analyzer, and light is transmitted. Without a light interaction with resonant atoms, the transmitted intensity is zero. The transmitted CFS intensity is approximately proportional to the square of the number density of the atoms.

The CFS and AA spectra of an Ar I 842.5-nm line in pulsed RF GD plasma were recorded using a CFS spectrometer in a Faraday configuration with permanent double-ring magnets and a diode laser source. Zeeman splitting of the conventional AA spectrum and the self-absorption profile of CFS radiation could be observed for different magnetic fields of above ~ 50 and ~ 10 mT, respectively. This might be explained by assuming that the CFS radiation consists of left- and right-handed circularly polarized radiation for higher and lower off-resonance frequencies, respectively. Based on the simulated absorption profiles, Zeeman splitting can be observed at above ~ 50 mT for a conventional AA signal and below ~ 10 mT for the self-absorption of CFS radiation [1].

Because the presence of a magnetic field does not require observation of an AA signal, the measured profile provides information regarding the location of the highest number density of the excited argon atoms in the lower state of the Ar I 842.5-nm transition. In contrast, the self-absorption profile of the CFS radiation provides information regarding the location of the second-highest number density. This is because CFS radiation is generated when a magnetic field and the highest number density of the measured atoms both occur. This CFS radiation operates as a light source for the subsequent AA at the location of the second-highest number density.

The magnetic field determined by the measured Zeeman splitting (Fig. 1) and a calculation of the axial variation of the magnetic field of the GD tube (Fig. 2)

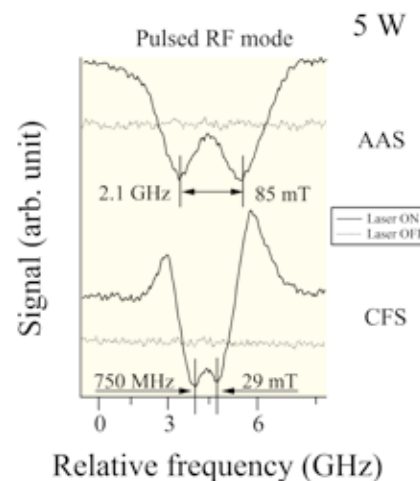


Fig. 1 Conventional AA spectrum and the self-absorption profile of CFS radiation at an RF power of 5 W

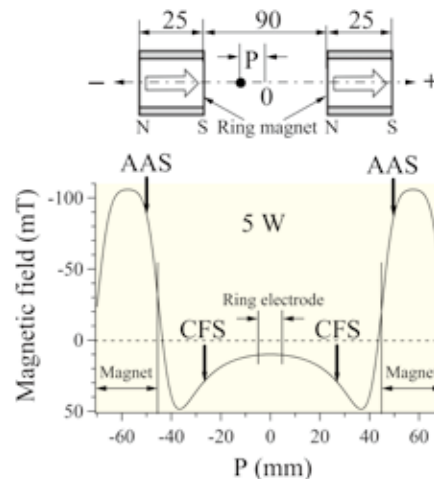


Fig. 2 Axial variation of the magnetic field and the position of the magnetic field determined from the AA and CFS profiles

allowed us to determine the locations of the highest and second-highest relative maximum number density of the excited argon atoms in the lower state of the Ar I 842.5-nm transition.

References

- [1] H. Matsuta, *Spectrochim. Acta Part B* **149**, 150 (2018).

Fatigue Improvement of Biomedical Co-Cr-Mo Alloy Fabricated by Using Electron Beam Melting

Biomedical Co-Cr-Mo alloys fabricated using additive manufacturing techniques generally exhibit relatively non-uniform microstructures and poor mechanical properties. Herein, we modified the microstructures and enhanced the fatigue properties of Co-Cr-Mo alloy fabricated through electron beam melting by utilizing an accessible post production heat treatment regime, which provides an avenue for improving the serviceability of the additive manufactured metallic components.

Biomedical Co-Cr-Mo alloys are widely used in orthopedic implants such as artificial knee and hip joints. In contrast, electron beam melting (EBM), a layer-by-layer additive manufacturing technique, has been utilized for fabricating near-net-shaped metallic components with complex shapes and geometries. However, the non-uniform microstructures and mechanical properties are the main drawbacks constraining the serviceability of as-EBM built components.

We recently demonstrated the microstructural characteristics of as-built biomedical Co-Cr-Mo alloys [1], and subsequently improved the fatigue properties based on manipulating the microstructure through an accessible post-production heat treatment regime [2]. The as-built γ/ε dual phase structures were selectively transformed into a predominant ε phase by ageing at 800 °C for 12 h, and then reverse transformed into a predominant γ phase by further ageing at 1000 °C for 10 min. As a result, both stress- and strain-controlled fatigue properties were improved, as illustrated in Fig. 1.

Figure. 2 shows STEM images demonstrating the microstructures of the as-built (Fig. 2a), HT (Fig. 2b), and RT (Fig. 2c) specimens after applying stress-controlled fatigue until failure. Bands or laths of the ε -phase were formed in the γ matrix of the as-built and reverse-transformed samples by means of a $\gamma \rightarrow \varepsilon$ strain-induced martensite transformation while under fatigue. This transformation is attributed to the motion of the partial Shockley dislocations on the alternative $\{111\}$ planes of the γ phase. However, a single ε -phase without a band structure was observed in the heat-treated sample, wherein the ε -matrix contained a high density of dislocations. This indicates that the fatigue proceeded mainly through plastic deformation of the ε -matrix. In the present study, the fatigue properties of as-EBM-built biomedical Co-Cr-Mo alloy were significantly

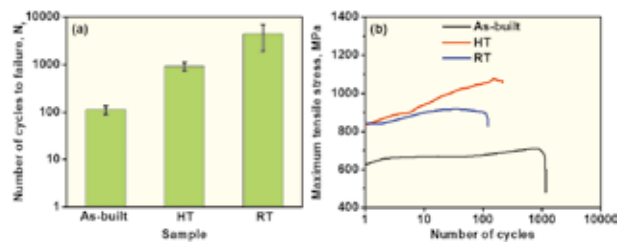


Fig. 1 (a) Number of cycles until failure under stress-controlled fatigue and (b) maximum tensile stress of strain-controlled fatigue of the as-EBM built, heat treated (HT), and reverse-transformed (RT) Co-Cr-Mo alloys.

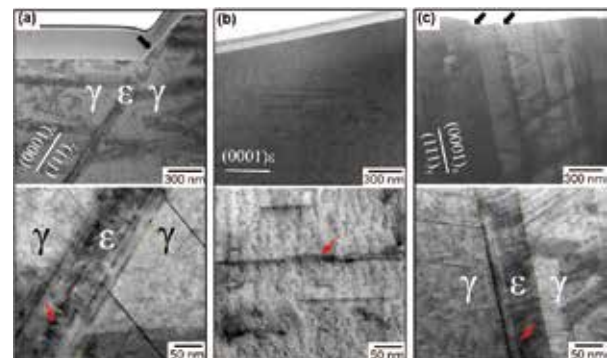


Fig. 2 STEM images showing microstructures of (a) as-EBM built, (b) heat-treated, and (c) reverse-transformed biomedical Co-Cr-Mo alloys after stress-controlled fatigue was applied until failure. The incident beam is parallel to $\{111\}_\gamma // (0001)_\varepsilon$.

improved by manipulating the fatigue deformation behaviors.

References

- [1] D. Wei, Y. Koizumi, A. Chiba, K. Ueki, K. Ueda, T. Narushima, Y. Tsutsumi, and T. Hanawa, *Additive Manuf.* **24**, 103 (2018).
- [2] D. Wei, Y. Koizumi, T. Takashima, M. Nagasako, and A. Chiba, *Mater. Res. Lett.* **6** (1), 93 (2018).

Keywords: microstructure, mechanical properties, fatigue

Daixiu Wei (Creation of Life Innovation Materials for Interdisciplinary and International Researcher Development)

E-mail: wei1987xiu@imr.tohoku.ac.jp

Hidemi Kato (Leader of Creation of Life Innovation Materials for Interdisciplinary and International Researcher Development)

E-mail: hikato@imr.tohoku.ac.jp

URL: <http://life-pro.imr.tohoku.ac.jp/index.html>

Development of Integrated Education Program for Young Researchers in Computational Materials Science

Professional development Consortium for Computational Materials Scientists (PCoMS) supports young researchers in the area of computational materials science (CMS) to develop their broader view and extensive knowledge in interdisciplinary areas including materials science (MS), condensed matter physics, molecular science, and material design. A recent activity by key members of PCoMS is introduced. Professors Terada and Mohri are developing and assessing the integrated education program of “specialized CMS” and “training of human skills.”

More than 50 years have passed since research using supercomputers started in the field of materials science (MS). Progress in computational materials science (CMS) has recently accelerated the discovery of advanced and novel materials. However, there have been few quantitative analyses regarding the trend in the number of doctors in CMS in Japan. In addition, doctors in Japan have recently been expected to work not only in academia, but also in industry. However, doctors in non-academia are still limited. They are demanded to have not only high expertise, but also wide knowledge of MS and human skills as advanced industry experts. There are some mismatches between the required knowledge and skills of doctors in industry and the contents of education in CMS.

We estimated the change in the number of doctors in CMS in Japan during the last 50 years by analyzing the subjects of doctoral dissertations found in a Japanese doctoral dissertation database [1]. Figure 1 shows the changes in the new doctors of science and engineering (SE) at sixteen domestic research universities and the new doctors of CMS at the same universities during the last 50 years. The number of doctors in SE, which rapidly increased during the 1990s owing to a reconstruction of the graduate school, peaked at approximately 2000, and has since rapidly decreased owing to the recent birthrate decline in Japan. In contrast, the number of doctors in CMS continued to increase until 2010, and the rate of decrease thereafter has been small. Consequently, the ratio of doctors in CMS to those in SE has continued to increase, exceeding 0.07 in 2015. This indicates that the importance of researchers in CMS is increasing.

In general, CMS lectures and human skills trainings are given by experts independently. There are few students and young researchers actively participating in human skills trainings. Therefore, we developed and assessed an integrated education program of CMS and the training of human skills in supporting young researchers to overcome the gaps among fundamental research, applied research, and practical applications [2]. One of our unique elective courses is PCoMS three-day seminar. The main contents

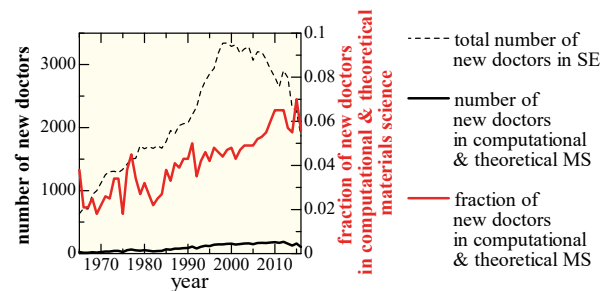


Fig. 1 Number of new doctors of 16 domestic research universities in Japan in last fifty years.

of this seminar are (1) lectures and practical computational training given by experts in both academia and industry, and (2) group discussions regarding research proposals related to both seminar topics and group member research topics. After seminars were conducted in 2016, 2017, and 2018, all 32 participants were emailed a link to a web survey. Among them, 24 of the participants answered the questionnaires. Based on the analysis of the questionnaire survey, we found that the satisfaction of the participants is high, although they think that a group discussion is a difficult task. Students and researchers typically do not have a sufficient chance to communicate with others in different research fields. After the discussion, they improved their human skills for communication with other students and researchers in different research fields, and came to understand the need for wide MS knowledge and human skills for scientific communication for interdisciplinary studies and innovation.

References

- [1] Y. Terada and T. Mohri, A study on trend of doctors in Japanese Computational Materials Science in last fifty years, JIM Annual Spring Meeting 2019, Mar. 20, 2019.
- [2] Y. Terada and T. Mohri, Integration of “specialized educational science lectures” and “training of human skills” and transferable skills” in computational materials science, SMS2018, P64, Abstracts of SMS2018, Oct. 30, 2018.

Keywords: computational materials science, higher education

Yayoi Terada (Professional development Consortium for Computational Materials Scientists)

E-mail: terada@imr.tohoku.ac.jp

Tetsuo Mohri (Project Leader of Professional development Consortium for Computational Materials Scientists)

URL: <http://pcoms.imr.tohoku.ac.jp/>

Energy-Related Materials

IMR KINKEN Research Highlights 2019



Self-Arrangement of Dislocations at Crystal/melt Interface During Directional Solidification of Silicon

The formation of small-angle grain boundaries (SAGBs) at a silicon crystal/melt interface during directional solidification was directly observed. Dislocations were demonstrated to self-arrange through polygonization into an energetically favorable SAGB configuration at the crystal/melt interface. The present results suggest that there is considerable dislocation motion at the solid/melt interface and that polygonization can occur during solidification.

The efficiency of solar cells manufactured using multicrystalline silicon (mc-Si) substrates is limited because of the various defects that exist in such material. Among the different types of GBs, small-angle GBs (SAGBs), which have a lower misorientation, have been confirmed to possess a high capability for impurity gettering. Studies on the relationship between the SAGB structure and the solar cell performance have found that a certain type of structural dislocation in SAGBs is responsible for an absolute performance loss of up to approximately 5%. Understanding the evolution of SAGBs during directional solidification would help in improving the quality of mc-Si substrates. In this study, we attempted to reveal the mechanisms behind the emergence and extension of SAGBs in mc-Si.

Figure 1 shows photographs taken during an *in situ* observation of the solidification of silicon [1]. The solidification rate ranges from 40 to 70 $\mu\text{m s}^{-1}$, which is moderately faster than the growth rate of industrial mc-Si (33.3 $\mu\text{m s}^{-1}$) while providing comparable conditions for observing the behavior of crystal growth. It is clearly shown that SAGBs, which appear as white lines almost perpendicular to the solid/melt interface, are propagating along the growth direction. The emergence of new SAGBs was observed at the moving crystal/melt interface.

Figure 2 shows photographs of areas taken through an *in situ* observation of the directional solidification and using an SEM after crystallization [1]. The places of origin of the SAGBs, as observed through an SEM after Sopori etching, are shown. The dislocations aggregate and exhibit a linear arrangement during solidification.

Polygonization of the dislocations in various materials has been extensively investigated; however, little attention has been paid to a crystal/melt interface. In this study, we directly observed the formation of SAGBs at a crystal/melt interface. The results indicate that the dislocation motion at

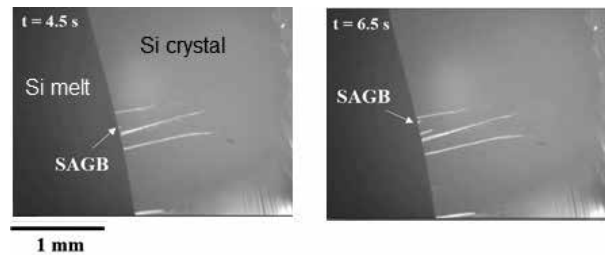


Fig. 1 Emergence of SAGBs at a moving crystal/melt interface.

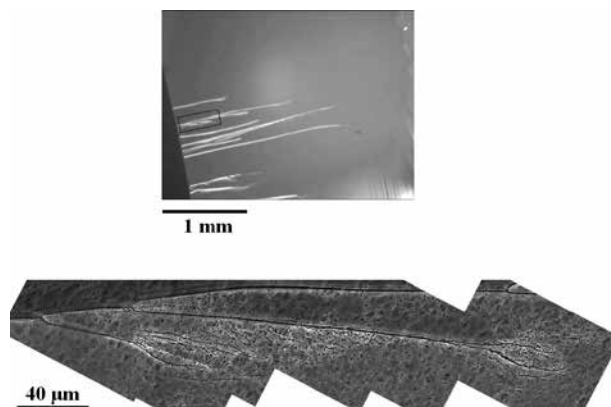


Fig. 2 Etch pit distributions before and after SAGB formation.

the crystal/melt interface is extremely active. The present results clearly show that the formation of SAGBs occurs at a crystal/melt interface during directional solidification, not only during the cooling process after solidification.

References

- [1] L.-C. Chuang, K. Maeda, H. Morito, K. Shiga, and K. Fujiwara, *Materialia* **3**, 347 (2018).

Materials Design for Super-Precise System Based on Molecular Dynamics Simulation

Recent materials design for super-precise systems strongly requires a deep understanding of multi-physics phenomena, including the chemical reactions, friction, impact, fluid, and heat. We applied our multi-physics computational simulator based on a molecular dynamics method and revealed the multi-physics phenomena that contribute to the materials design in the mechanical engineering field such as solar cells, electronics, tribology etc.

High-functional and high-performance materials are necessary in a wide variety of research fields, such as solar cells, electronics, tribology etc., to develop super-precision systems. For the materials design, we need a deep understanding of the multi-physics phenomena, including the chemical reactions, friction, fluid, and heat. However, traditional simulation methods such as fluid mechanics and first-principle calculations cannot simulate the multi-physics phenomena. Thus, we applied our multi-physics simulators based on classical molecular dynamics (MD), tight-binding quantum chemical MD, first-principles MD, etc., for pioneering next-generation materials design [1-3].

An ionic liquid (IL)-assisted vacuum deposition method has recently been introduced for the fabrication of single-crystal pentacene for organic solar cells and organic electronic devices. This experimental study suggested that a higher diffusion of IL tends to provide a higher quality of the pentacene crystal. We thus investigated the diffusion coefficient of ions in a thin-film ionic liquid (TF-IL)-on α -Al₂O₃(0001) through MD simulations (Fig. 1a) [1]. The simulation results show that the diffusion coefficient in a 2 nm thin-film is significantly lower than that at other thicknesses (Fig. 1b) because the layered structure of ILs is formed on the substrate. We suggest that the TF-IL thickness should be above the layered structure to avoid a low diffusion coefficient and low quality of pentacene crystal in IL-assisted vacuum deposition.

Diamond-like carbon (DLC) is a promising solid lubricant used to reduce the friction against α -Al₂O₃. The friction of DLC/ α -Al₂O₃ strongly depends on temperature. To reveal the friction mechanism, we investigate the friction behaviors of DLC/ α -Al₂O₃ at various temperatures using our developed tight-binding quantum chemical MD simulator [2]. Interestingly, the volcano-type temperature dependence of the friction coefficients is observed (Fig. 2a). At 300–600 K, DLC/ α -Al₂O₃ shows smooth sliding. However, at 600–800 K, interfacial C–O and C–Al bonds are generated, and the friction coefficients increase. Over 800 K, the number of interfacial bonds

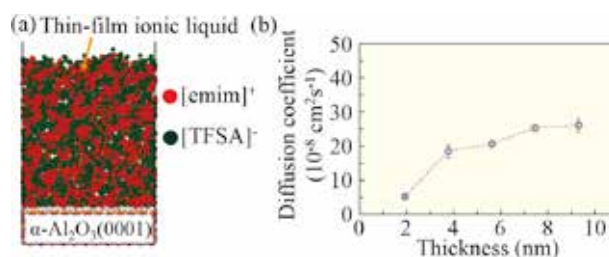


Fig. 1 (a) Schematic of a thin-film ionic liquid (TF-IL) on α -Al₂O₃(0001) substrate. (b) Self-diffusion coefficient in the out-of-plane direction.

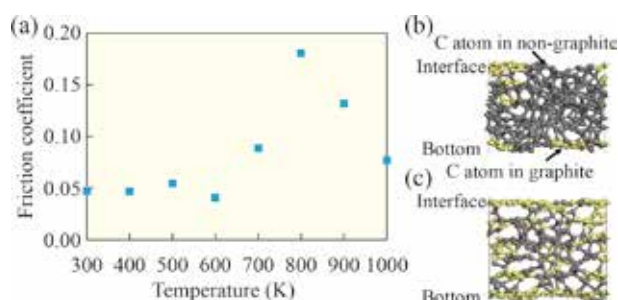


Fig. 2 (a) Friction coefficients of DLC/ α -Al₂O₃ at each temperature. DLC film structures (b) before and (c) after friction at 800 K.

and friction coefficients decrease. It is interesting to note that chemically stable graphite is formed on the DLC surface during the friction at 800 K (Fig. 2b, c), and inhibits the interfacial bond generation. We revealed the unique friction mechanism of DLC/ α -Al₂O₃ owing to the structural changes in the friction interface through the multi-physics phenomena of the chemical reaction, friction, and heat.

References

- [1] S. Maruyama, I.B.H. Pratiawan, K. Toyabe, Y. Higuchi, T. Koganezawa, M. Kubo, and Y. Matsumoto, *ACS Nano* **12**, 10509 (2018).
- [2] Y. Wang, J. Xu, J. Zhang, Q. Chen, Y. Ootani, Y. Higuchi, N. Ozawa, J. M. Martin, K. Adachi, and M. Kubo, *Carbon* **133**, 350 (2018).
- [3] Y. Ootani, J. Xu, T. Hatano, and M. Kubo, *J. Phys. Chem. C* **122**, 10459 (2018).

Keywords: simulation, molecular dynamics, interface

Momiji Kubo (Materials Design by Computer Simulation Research Laboratory)

E-mail: momoji@imr.tohoku.ac.jp

URL: <http://www.simulation.imr.tohoku.ac.jp/>

Chemical State Mapping of Be₁₂Ti and Be₁₂V Beryllides by Soft X-Ray Emission Spectrometry

Be-rich intermetallics (beryllides) have been expected to be adopted for high-temperature environments, such as fusion reactors and gas turbines. Here, the chemical state micromapping of Be₁₂M (M = Ti,V) is shown based on the valence electron structure revealed using an electron probe microanalyzer with a novel soft X-ray emission spectroscope.

Beryllides have a great potential to be used in industrial applications for high-temperature environments, including structural materials for aerospace systems and refractory materials, because of their high strength and light weight. Recently, Be-rich intermetallics, such as Be₁₂M (M = Ti,V), have been expected to be neutron multipliers for fusion reactors as a substitute for pure metallic Be because of their significant advantage in oxidation resistance at elevated temperatures.

Elemental microanalysis by measuring a characteristic X-ray with electron microscopy is an essential approach in the development of oxidation-resistant beryllides. However, low-Z (Z: atomic number) elements such as Be (Z = 4) are difficult to detect by the conventional approaches using energy- and wavelength- dispersive spectrometers (EDS and WDS) for electron microscopy. Thus, a novel soft X-ray emission spectrometer (SXES) attached to an electron probe microanalyzer was used, which covers a low energy range (50-210 eV) with ultrahigh-energy resolutions of 0.22 eV for obtaining the chemical state map of the low-Z

elements such as boron [1] and beryllium.

The Be–K spectra from the Be₁₂M phases show significantly lower densities of the occupied states near the Be–K edge than those of metallic pure beryllium. Density functional theory calculations indicate that changes in the valence electron structure are derived from the large downward shift of the Fermi level in Be₁₂M, by at least 0.8 eV. Based on the knowledge of the valence electron structures and the chemical shift, chemical-state mappings of BeO and Be₁₂V in the oxidized beryllide specimen were successfully obtained, as shown in Fig. 1 [2].

The present approach is applicable for visualization and identification of metallic/oxidized phase in light-element compounds by an electron microscope.

References

- [1] R. Kasada, Y. Ha, T. Higuchi, and K. Sakamoto, *Sci. Rep.* **6**, 25700 (2016).
- [2] K. Mukai, R. Kasada, K. Yabuuchi, S. Konishi, J.-H. Kim, and M. Nakamichi, *ACS Applied Energy Mater.* **2**, 2889 (2019).

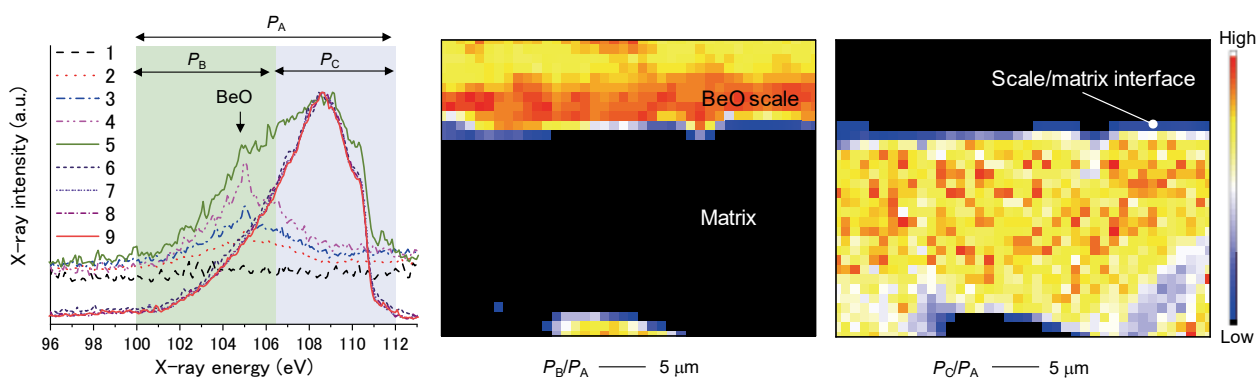


Fig. 1 Be–K spectra (left) by the SXES from nine measuring areas of the steamed Be₁₂V specimen: reconstructed images by calculating the peak area ratio of P_B/P_A and P_C/P_A , showing chemical-state mappings of BeO (center) and Be₁₂V (right) [2]

Keywords: nuclear materials, electronic structure, electron microscopy
 Ryuta Kasada (Nuclear Materials Engineering Research Laboratory)
 E-mail: r-kasada@imr.tohoku.ac.jp
 URL: <http://web.tohoku.ac.jp/imr-numat/>

Locations of Mn and Fe in Andalusite from Västanaåberget, Sweden

Local structural features around Mn and Fe in Mn-bearing andalusite from Västanaåberget, Sweden, were investigated by anomalous X-ray scattering (AXS) and X-ray absorption fine structure (XAFS) spectroscopy. The elemental distribution map of Mn obtained by AXS and the extended X-ray absorption fine structure (EXAFS) spectra indicate that Mn atoms exclusively occupy the Al1 sites. EXAFS analyses reveal that Fe occupies both Al1 and Al2 sites. Utilizing the local structural information around Mn and Fe, a conventional single-crystal structural refinement converges at $R = 2.34\%$, with a structural formula of $(\text{Al}_{0.82}\text{Mn}_{0.16}\text{Fe}_{0.02})^{[6]}(\text{Al}_{0.99}\text{Fe}_{0.01})^{[5]}\text{SiO}_5$.

Mn-bearing andalusite has a structural formula of $(\text{Al}_{2-x-y}\text{Mn}_x\text{Fe}_y)\text{SiO}_5$. The stability and optical properties of andalusite strongly depend on the substitution of transition metals and their coordination environments, as shown in Fig. 1. In general, presence of even a small amount of Mn and the coexisting Fe lead to uncertainties in the modeling of the site preferences for two distinct Al sites, when only conventional single-crystal X-ray diffraction (XRD) data are considered. Herein, we report direct evidence for the site preferences of Mn and Fe in andalusite using anomalous X-ray scattering (AXS) and X-ray absorption fine structure (XAFS) spectroscopy.

To revise the structural model, results of the AXS analysis were used. Figure 2 shows the distribution maps of Mn at $z = 0$ and 0.25 obtained by a difference Fourier synthesis of the Mn AXS data. The distribution of Mn is observed exclusively at the Al1 site. This result suggests a strong preference of Mn for the Al1 site. Similarly, the distribution map for Fe indicates that Fe occupies both Al1 and Al2 sites. Based on these results, we were able to improve the structural model.

During the XANES analysis of the local structure of Mn and Fe, we employed a multiple-scattering simulation method using the structural parameters obtained by single-crystal XRD. These data support the observation that Mn exclusively occupies the Al1 site. Furthermore, a distorted octahedron is deduced from the bond distances obtained at 1.87–2.26 Å, and the average value of $\langle \text{Mn-O} \rangle = 2.03$ Å suggests the Jahn–Teller distortion of the Mn^{3+}O_6 octahedra. Notably, the $\langle \text{Mn-O} \rangle$ distance is comparable to the distance between the Al1 site and O atom in kanonaite, which is fully occupied by Mn and Fe atoms. This result indicates that the local Mn–O bond distances in andalusite are comparable to those of kanonaite regardless of the Mn content. This phenomenon is known as complete structural relaxation, where Mn retains its atomic size. These local structures around Mn suggest strong

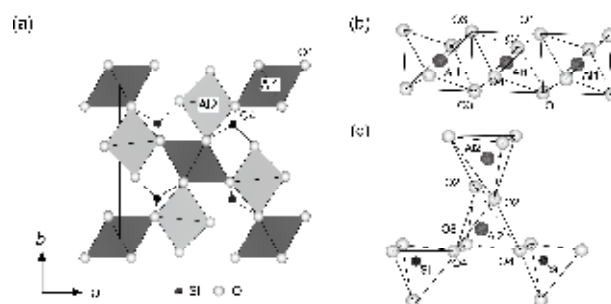


Fig. 1 Crystal structure of the Mn-bearing andalusite from Västanaåberget, Sweden, and coordination environments of the Al1 and Al2 sites.

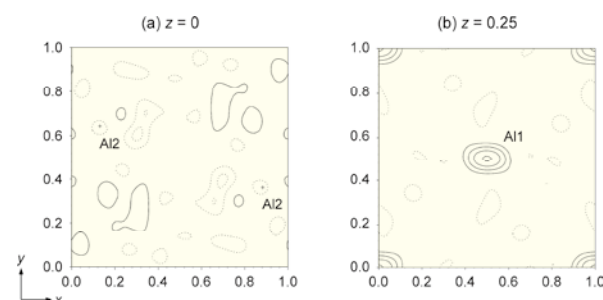


Fig. 2 Mn distribution maps at (a) $z = 0$ and (b) $z = 0.25$ obtained by AXS measurement at the Mn K-absorption edge.

correlation to the Mn-site preference and maximum possible Mn content in the andalusite structure. The recent first-principles study by Wang et al. (2017) shows that a large number of Mn atoms can occupy Al1 sites due to the large Jahn–Teller distortion of Mn^{3+}O_6 octahedra and low bulk modulus of the andalusite phase, which further suggests the structural relaxation phenomenon discussed previously. However, the EXAFS spectrum of Fe is not reproduced by the simulated models derived by substituting the atoms in Al1 or Al2 sites with an Fe atom.

References

- [1] H. Arima, Y. Tani, K. Sugiyama, and A. Yoshiasa, *J. Min. Pet. Sci.* **113**, 273 (2018).

Keywords: XAFS, XRD, synchrotron

Hiroshi Arima (Chemical Physics of Non-Crystalline Materials Research Laboratory)

E-mail: h_arima@cross.or.jp

URL: <http://www.imr.tohoku.ac.jp/en/about/divisions-and-centers/research-division/15.html>

Fast Diffusion of Multivalent Ions in Cathode Materials Facilitated by Concerted Interaction with Monovalent Ions — A Perspective on Constructing Novel Rechargeable Batteries with Safety & High-Energy Density

We are currently constructing a new type of rechargeable battery using divalent Mg cations. We determined through electrochemical experiments combined with first-principles calculations that the diffusion of divalent Mg ions, whose diffusion in cathode materials is usually sluggish, is dramatically facilitated by the concerted interaction between Mg and monovalent Li ions.

In terms of energy and environmental concerns, modern industrial society strongly demands high energy-density rechargeable storage batteries. Lithium ion batteries (LIBs) are being widely used for a number of practical applications, although their performance is gradually approaching the theoretical limit. If lithium metal itself could be used as an anode material instead of the currently used carbonaceous materials, LIBs would have demonstrated significantly high energy densities; however, this is difficult owing to the notorious problem of “dendritic growth” of Li metal during a charge, which leads to a dangerous short circuit.

As an alternative to a Li metal-anode battery, multivalent-ion (Mg^{2+} , Zn^{2+} , Al^{3+} , etc.) batteries have attracted attention because a safe and high-capacity metal can be employed as an anode material; for example, in the case of Mg, its capacity ($\sim 2,200 \text{ mAhg}^{-1}$) largely exceeds that of current carbonaceous anode materials ($\sim 370 \text{ mAhg}^{-1}$). However, the diffusion of multivalent ions in cathode materials is known to be typically sluggish, which causes an increase in the overpotential.

Because these problems are difficult to be solved in a single-carrier ion battery system, we designed a new battery technology utilizing both Li and Mg ions,

which we refer to as a Li-Mg dual-cation battery [1]. We experimentally confirmed that the co-electrodeposition of Li-Mg dual cations can significantly suppress Li dendritic growth, and that the concomitant intercalation of both ions into a Mo_6S_8 Chevrel or MgCo_2O_4 spinel cathode occurs in Li-Mg dual-cation batteries with a much lower overpotential than that in a Mg single-carrier ion battery [1]. This indicates that divalent Mg ion diffusion is promoted by the presence of monovalent Li ions in a cathode.

We elucidated through first-principles calculations that the activation energy of Mg diffusion in Mo_6S_8 is reduced remarkably in a Li-Mg dual-cation system by the “concerted” motion of the following Mg and leading Li ions with the Li-Mg distance remaining nearly constant, as shown in Fig. 1 [2]. This proves that dual-ion systems are a promising way to construct novel high-performance rechargeable batteries employing multivalent ions with an enhanced diffusion rate.

References

- [1] H. Li, T. Ichitsubo, S. Yagi, and E. Matsubara, *J. Mater. Chem. A* **5**, 3534 (2017).
- [2] H. Li, N. L. Okamoto, T. Hatakayama, Y. Kumagai, F. Oba, and T. Ichitsubo, *Adv. Energy Mater.* **8**, 1801475 (2018).

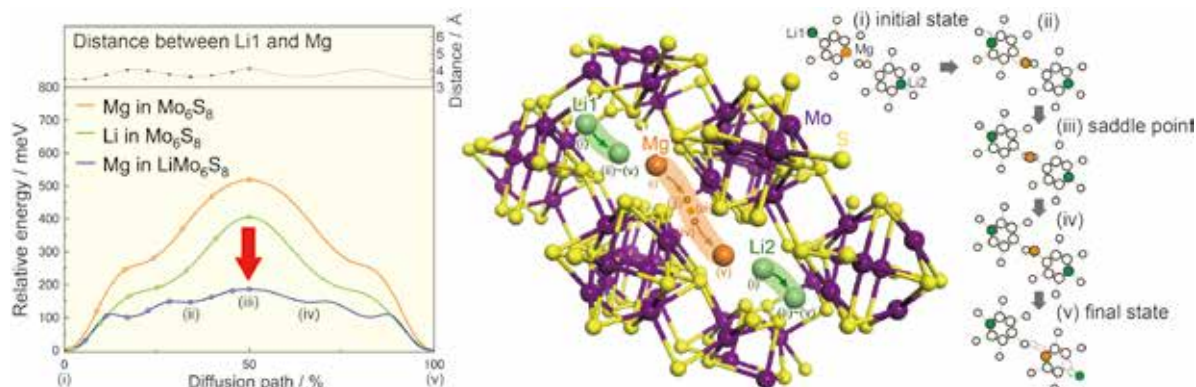


Fig. 1 (a) Activation energies computed using the nudged elastic band method for the diffusion processes. (b) Schematic figure illustrating the minimum energy diffusion path of Mg ions in a LiMo_6S_8 host.

Keywords: energy storage, crystal structure, diffusion

Tetsu Ichitsubo, Norihiko L. Okamoto, Hiroshi Tanimura, and Tomoya Kawaguchi (Structure-Controlled Functional Materials Research Laboratory)

E-mail: tichi@imr.tohoku.ac.jp

URL: <http://ilab.imr.tohoku.ac.jp/index.html>

Investigation of Structure and Properties of Nano and Submicrometer Porous Metals Formed by Liquid Metal Dealloying

The liquid metal dealloying (LMD) technique facilitates preparation of fine porous materials with base metal elements, which is difficult to achieve by means of the conventional chemical dealloying techniques. In this study, the mechanism of morphology formation during LMD was studied by scanning electron microscopy, X-ray diffraction, electron backscatter diffraction, and X-ray and electron tomography.

Nano and submicrometer porous metals have attracted considerable attention for their excellent functional properties. The most promising technique used to prepare such porous metals is dealloying in aqueous solution. Nanoporous noble metals including Au have been prepared from binary alloy precursors. The less noble metals, unstable in aqueous solution, are oxidized immediately when they contact water at a given potential, so this process is only possible for noble metals. Porous structures with less noble metals, such as Ti or Fe, are highly desired for various applications, including energy-harvesting devices. To overcome this limitation, a liquid metal dealloying (LMD) was developed at the Kato Lab. LMD is a selective dissolution phenomenon of a mono-phase alloy solid precursor: one component (referred to as a “soluble component”) is soluble in the metallic melt, while the other (referred to as the “targeted component”) is not. When the solid precursor contacts the metallic melt, only atoms of the soluble component dissolve into the melt, inducing a spontaneously organized bicontinuous structure at a microstructure level. The LMD has enabled the preparation of nano and submicrometer porous structures in less noble metals, such as Ti, Ni, Si, Fe, Nb, Co, and Cr. In this study, the mechanism of morphology formation during the LMD process was three dimensionally analyzed *in situ* and *ex situ* using X-ray tomography [1].

Figure 1(a) shows a scanning electron microscopy (SEM) image and reconstructed 3D structure (inset) of porous Fe-Cr alloy prepared from a Fe₄₀Cr₁₀Ni₅₀ (at.%) precursor. Two phases (metal and air) can be clearly distinguished in the reconstructed 3D image. This 3D morphological analysis made it possible to evaluate quantitatively the volume fraction of phases, surface area, connectivity, and tortuosity more precisely than with the 2D analyses done previously. Figure 1(b) shows the experimental setup for 3D observation of the dealloying process *in situ*. The LMD cell was put

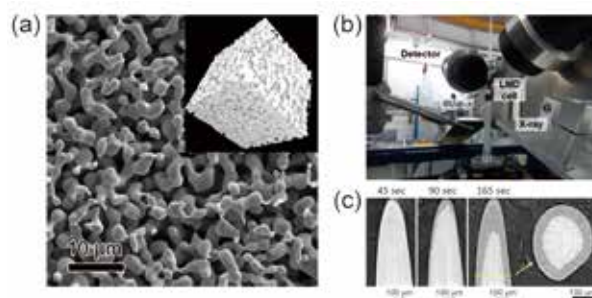


Figure 1 (a) SEM image and reconstructed 3D structure (inset) of porous Fe–Cr alloy prepared from Fe₄₀Cr₁₀Ni₅₀ precursor, (b) experimental setup for 3D *in situ* observation of dealloying in the ESRF beam line and (c) evolution of porous metal layer by LMD in the Fe₄₀Cr₁₀Ni₅₀ needle precursor in the longitudinal cross section at different reaction times of 45, 90, and 165 s — the transverse cross section image at 165 s is also shown

into the intense X-ray beam line at the European Synchrotron Radiation Facility (ESRF). The cell was heated by the laser, and a tomogram image was acquired. The bottom of Fig 1(c), shows the evolution of the porous metal layer in Fe₄₀Cr₁₀Ni₅₀ needle precursor at 45, 90, and 165 s. The dark area and bright area in the needle sample correspond to dealloyed porous metal and an undealloyed layer, respectively. The thickness of the porous metal layer linearly increases with time, indicating that the dealloying reaction kinetic was controlled by the interfacial reaction in this cell.

References

- [1] M. Mokhtari, C. L. Bourlot, J. Adrien, A. Bonnin, T. Wada J. Duchet-Rumeauc, H. Kato, and E. Maire, *Mater. Charact.* **144**, 166 (2018).

Keywords: foam, porosity, 3D structure

Hidemi Kato (Non-Equilibrium Materials Research Laboratory)

E-mail: hikato@imr.tohoku.ac.jp

URL: <http://www.nem2.imr.tohoku.ac.jp/>

Visualization of Anomalous Ettingshausen Effect in an FePt Ferromagnetic Thin Film

The anomalous Ettingshausen effect (AEE) is one of the well-known thermoelectric effects in ferromagnets, although only a few studies on AEE have been reported for bulk materials. Here, we show a visualization of the temperature modulation owing to the AEE in an FePt ferromagnetic thin film by utilizing a lock-in thermography technique.

Interconversion between an electric charge current (J_c) and a heat current (J_q) mediated by a spin current (J_s), which has frequently been called “spin-caloritronics” [1], has fascinated researchers ever since the progress made in energy harvesting has necessitated a new route toward a highly efficient thermoelectric conversion. The anomalous Nernst effect (ANE) and anomalous Ettingshausen effect (AEE) are well-known thermoelectric phenomena, in which the coexistence of magnetization (M) and the temperature gradient (∇T) produces an anomalous Nernst voltage, whereas that of J_c and M leads to ∇T owing to the AEE. The ANE has been widely studied for various types of ferromagnetic bulks and thin films. In contrast to the ANE, there have been no reports on the AEE in a ferromagnetic thin film, although a few studies on the AEE in ferromagnetic bulks have been reported. When a heating/cooling device based on the spin-caloritronic phenomena is designed, the detailed spatial distribution of the temperature modulation in a reduced dimension needs to be known.

Herein, we report the observation of the AEE in a ferromagnetic thin film [2, 3]. We chose FePt alloy as a material for visualizing the AEE. A 10-nm thick FePt (100) film was epitaxially grown on a SrTiO₃ (100) substrate at 350 °C using an ultrahigh vacuum magnetron sputtering system. For thermal imaging of the AEE, the lock-in thermography (LIT) technique was used. The infrared radiation thermally emitted from the sample surface was detected while applying rectangular-wave modulated J_c to a U-shaped FePt (Fig. 1(a)). Only the first harmonic response was fed to separate the AEE from the Joule heating.

Figure 1(b) shows the amplitude (A) and phase (ϕ) images of the temperature modulation for the in-plane magnetized FePt. An increase in A appears in the y -directional wires with the opposite ϕ in the right and left wires. This means that the sign of the temperature modulation is reversed when reversing the vector product of M and J_c . The spatial

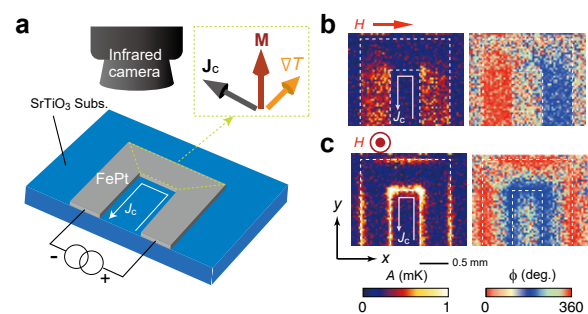


Fig. 1 (a) Schematic illustration of U-shaped FePt along with the lock-in thermography setup. The relationship between charge current (J_c) and temperature gradient (∇T) for the perpendicular magnetization (M) is also shown. (b) Amplitude (A) and phase (ϕ) images of temperature modulation for the in-plane and (c) perpendicularly magnetized FePt.

distribution of the temperature modulation is completely changed by changing the FePt magnetization from in-plane to out-of-plane. Figure 1(c) shows the thermal image of the perpendicularly magnetized FePt. Clear A signals appear around the edges of the U-shaped wire, and the ϕ difference between the inside and outside edges is $\sim 180^\circ$.

These temperature modulations are well understood by considering the symmetry of the AEE. In addition, our numerical calculation suggests that the different distribution of the heat sources for the in-plane and perpendicularly magnetized FePt lead to different temperature profiles of the AEE for a thin-film structure, which is an important finding in the design of spin-caloritronic devices.

References

- [1] S. R. Boona, R. C. Myers, and J. P. Heremans, *Energy Environ. Sci.* **7**, 885 (2014).
- [2] T. Seki, R. Iguchi, K. Takanashi, and K. Uchida, *Appl. Phys. Lett.* **112**, 152403 (2018).
- [3] T. Seki, R. Iguchi, K. Takanashi, and K. Uchida, *J. Phys. D: Appl. Phys.* **51**, 254001 (2018).

Keywords: magnetic properties, thermo-electricity, thin films
 Koki Takanashi (Magnetic Materials Research Laboratory)
 E-mail: koki@imr.tohoku.ac.jp
 URL: <http://magmatelab.imr.tohoku.ac.jp/>

Intermediate Hydrogen States in the Formation Process of a Complex Transition Metal Hydride

The hydrogen states during the formation process of a complex transition metal hydride $\text{LaMg}_2\text{NiH}_7$ composed of La^{3+} , Mg^{2+} , $[\text{NiH}_4]^{4-}$, and H^- was investigated, which is indispensable to obtain guideline for designing high hydrogen density storage materials. The results indicate the presence of intermediate hydrogen states prior to the formation of $[\text{NiH}_4]^{4-}$ and H^- .

Complex transition metal hydrides composed of metal cations (e.g. Mg^{2+}) and complex anions (e.g., $[\text{NiH}_4]^{4-}$ with covalent hydrogen ($\text{H}^{\text{cov.}}$)) are attractive for use in energy-related materials such as hydrogen storage materials. The formation process of hydrogen states in compounds is therefore important because hydrogen exhibits various states, which are interstitial hydrogen (H^0), proton (H^+), hydride ion (H^-), and $\text{H}^{\text{cov.}}$, and related with designing high hydrogen density storage materials. Focusing on a complex transition metal hydride, $\text{LaMg}_2\text{NiH}_7$ composed of La^{3+} , Mg^{2+} , $[\text{NiH}_4]^{4-}$, and H^- , we clarified the formation process of $\text{LaMg}_2\text{NiH}_7$ studied using powder neutron diffraction (PND) and inelastic neutron scattering (INS).

Using PND, $\text{LaMg}_2\text{NiH}_7$ was revealed to form through an interstitial hydride $\text{LaMg}_2\text{NiH}_{0.05}$ with H^0 and an intermediate hydride $\text{LaMg}_2\text{NiH}_{4.6}$ with maintaining of local atomic arrangements (Fig. 1) [1, 2]. In $\text{LaMg}_2\text{NiH}_{4.6}$, hydrogen atoms were located around Ni with the formation of NiH_2 and NiH_3 units and in tetrahedral sites (T-site).

To identify the hydrogen states in NiH_2 and NiH_3 units and H in T-sites in $\text{LaMg}_2\text{NiH}_{4.6}$, hydrogen vibrations in $\text{LaMg}_2\text{NiH}_{4.6}$ (Fig. 2) and $\text{LaMg}_2\text{NiH}_7$ were studied using the INS [3]. The results indicate that hydrogen atoms in NiH_2 and NiH_3 units in $\text{LaMg}_2\text{NiH}_{4.6}$ are covalently bound with Ni due to the observation of a H–Ni–H deformation and Ni–H stretching modes. However, the NiH_2 and NiH_3 units are not complex anions as $[\text{NiH}_4]^{4-}$ due to the lack of NiH_2 and NiH_3 libration modes. Furthermore, a wavenumber range of hydrogen vibrations in the T-sites in $\text{LaMg}_2\text{NiH}_{4.6}$ is between H^0 and H^- . The INS results suggest the presence of intermediate hydrogen states in $\text{LaMg}_2\text{NiH}_{4.6}$ prior to the formation of $[\text{NiH}_4]^{4-}$ and H^- . Thus, NiH_2 and NiH_3 units and hydrogen atoms in the T-sites have been suggested as precursors for $[\text{NiH}_4]^{4-}$ and H^- in $\text{LaMg}_2\text{NiH}_7$.

References

[1] K. Miwa, T. Sato, M. Matsuo, K. Ikeda, T. Otomo, S. Deledda,

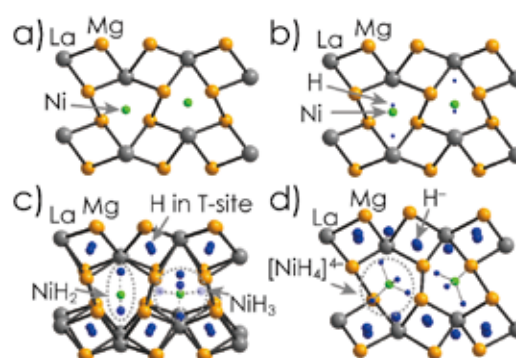


Fig. 1 Local atomic arrangements of (a) LaMg_2Ni , (b) $\text{LaMg}_2\text{NiH}_{0.05}$, (c) $\text{LaMg}_2\text{NiH}_{4.6}$, and (d) $\text{LaMg}_2\text{NiH}_7$. Grey, orange, green, and blue circles indicate La, Mg, Ni, and H, respectively.

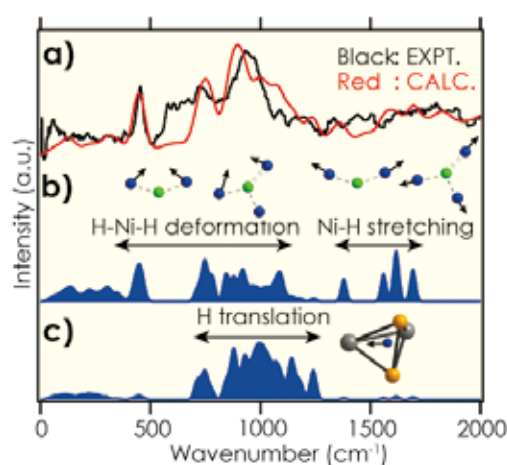


Fig. 2 (a) Experimentally observed and calculated INS spectra of $\text{LaMg}_2\text{NiH}_{4.6}$, and calculated contributions of H atoms in (b) NiH_2 and NiH_3 and (c) T-sites. Insets are schematic figures of H vibrations in NiH_2 , NiH_3 , and T-sites.

B. Hauback, G. Li, S. Takagi, and S. Orimo, *J. Phys. Chem. C* **120**, 5926 (2016).

[2] T. Sato, K. Ikeda, M. Matsuo, K. Miwa, T. Otomo, S. Deledda, B. Hauback, G. Li, S. Takagi, and S. Orimo, *Int. J. Hydrogen Energy* **42**, 22449 (2017).

[3] T. Sato, A. J. Ramirez-Cuesta, L. L. Daemen, Y. -Q. Cheng, and S. Orimo, *Inorg. Chem.* **57**, 867 (2018).

Keywords: hydride, crystal structure, neutron scattering

Toyoto Sato and Shin-ichi Orimo (Hydrogen Functional Materials Research Laboratory)

E-mail: toyoto@imr.tohoku.ac.jp

URL: <http://www.hydrogen.imr.tohoku.ac.jp/index.html>

Electronic Materials

IMR KINKEN Research Highlights 2019



Theory of Topologically Nontrivial Spin-Wave Solitons

The formation of spin-wave solitons in static and dynamic (Floquet) analogs of the Haldane model is considered. The nonlinearity arising from the crystalline anisotropy and magnon–magnon interactions is essential for the formation of solitons. We can observe different phases of solitons due to the interplay with the topologically nontrivial band structure.

There has been a surge in the classification of topological phases of matter for electronic systems, which pertain to band structures with a global nontrivial quantized phase quantified by a Chern number. Topologically nontrivial spin-wave (magnons) phases can also be realized in periodically modulated magnetic systems, called magnonic crystals. Solitons are self-localized wave packets that exist by compensating the frequency dispersion with nonlinearity. We combine the idea of solitons and the nontrivial band structure in magnonic crystals to open new avenues for spintronic applications [1]. For instance, the spin-wave solitons presented here can serve as memory bits with two topologically distinct phases can transfer information locally to a proximity magnetic system.

We consider a honeycomb spin lattice, analogous to the Haldane model, which includes the nearest neighbor exchange interaction and a Dzyaloshinskii–Moriya spin-orbit interaction generated in a static or dynamic (induced by excitation) manner. The magneto-crystalline anisotropy and non-local magnon–magnon interactions contribute to the nonlinearities. We developed a self-consistent mean-field method to determine the soliton modes in the spin-wave band gap.

We identified several soliton phases depending on the crystalline anisotropy coefficient (K) and the input power (P_0), as illustrated in Fig. 1(a). For a given K , the system supports solitons above a critical power P_{c1} (green-dashed line). We also observe a second threshold, P_{c2} (red-dashed line), which we identified to be a topological phase change, viz. the inside and outside of the soliton have different topologies. It is well-established that the boundary between regions with different topological phases hosts robust edge modes. Indeed, the solitons above P_{c2} have a finite density of states of edge modes at this dynamic boundary. Figure 1(b) shows the topologies of the distinct classes of solitons that have been identified.

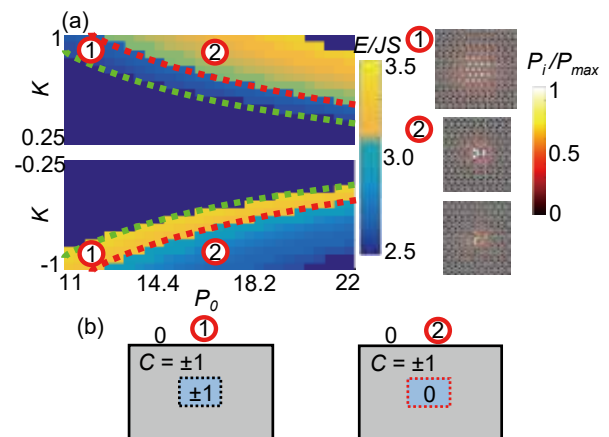


Fig. 1 (a) Soliton phase diagram in the parameter space of anisotropy constant K and power P_0 . In the dark-blue area, solitons do not form. The other colors indicate the calculated soliton energies E . ① and ② denote the distinct regions of the phase diagram. The right panels display the representative soliton density distributions found in ① (the top one) and ②. Green- and red-dashed lines mark the thresholds P_{c1} and P_{c2} , respectively. The right panels plot the soliton wave function intensity at each site P_i , normalized by the maximum in that panel P_{max} with the indicated color code. (b) The topology of solitons on the Haldane lattice below and above the threshold P_{c2} . The blue region is the soliton core that, at high intensities, has a different Chern number C from the rest of the lattice (embedded in a medium with $C = 0$).

Our findings provide interesting but challenging experimental results for magnetic 2D van der Waals materials, such as CrBr_3 , and magneto-dipolar magnonic lattices. Solitons found in our study and the corresponding topological classifications can serve as an information resource or as an experimental technique to reveal these novel magnonic edge modes.

References

- [1] M. Elyasi, K. Sato, and G. E. W. Bauer, Phys. Rev. B **99**, 134402 (2019).

Keywords: spin wave, spintronics

Mehrdad Elyasi, Koji Sato, and Gerrit Ernst-Wilhelm Bauer (Theory of Solid State Physics Research Laboratory)

E-mail: melyasi@imr.tohoku.ac.jp

URL: <http://www.bauer-lab.imr.tohoku.ac.jp/?page=&lang=en>

Quantum Critical Point of Charge Density Wave Ground State Is Found by Very High Magnetic Field X-ray Scattering with a 33-T Minicoil

The quantum critical point (QCP) hidden in the superconducting dome of underdoped hole-doped $\text{YBa}_2\text{Cu}_3\text{O}_x$ was examined by x-ray scattering experiment by combining a free electron laser with a unique high-field pulsed minicoil developed at the Institute for Materials Research. The charge density wave state, which has been found in very high magnetic fields, terminates at a doping concentration of 0.08. The breakdown of the translational symmetry was associated with the QCP.

In strongly correlated electron systems, such as high- T_c superconductors, a competition between localized and itinerant states is the source of their rich and complex phase diagrams. In underdoped $\text{YBa}_2\text{Cu}_3\text{O}_x$, in addition to the superconductivity at zero field, different phases, such as a spin density wave, an antiferromagnetic, pseudo gap, and low-field charge density wave (CDW) phases, have been found by tuning the system by chemical doping, temperature, pressure, and a high magnetic field. Because of those, the nature of the CDW phases is under intensive investigation.

Until the striking discovery that there appear two types of CDW state in low- and high-magnetic-field areas, the role of a high magnetic field is considered simply to suppress the superconductivity in a continuous manner. In contrast to this expectation, the three-dimensional (3D) CDW phase appears only in the high-magnetic-field regime, and it is different from the short-ranged two-dimensional CDW that appears in the pseudogap regime [1].

The next question is whether there is a terminating point of the 3D CDW phase along with the hole concentration. To clarify this point, a systematic study was conducted on x-ray scattering in very high magnetic fields of as much as 33 T in the hole concentration between 0.07 and 0.12. There are two experimental key points: one is the use of a high intensely pulsed x-ray source from the x-ray-free electron laser at the Linac Coherent Light Source at the Stanford National Accelerator Laboratory, and the other is the use of a compact minicoil developed at the Institute for Materials Research (IMR) that can generate 35-40-T-class pulsed magnetic fields.

Figure 1 shows a picture of a minicoil with an outer diameter of 30 mm. By using a compact pulsed power generator developed at the magnetism division at IMR, 40 and 50 T were available with a split-pair coil and a solenoid coil, respectively, as of 2018.

The determined hole concentration dependence of the 3D CDW signal is depicted in Fig. 1. The

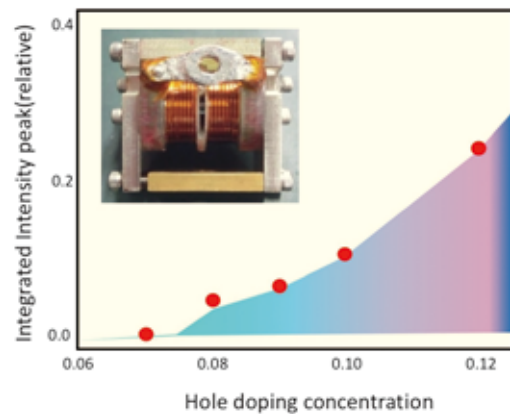


Fig. 1 IMR's mini-split-pair coil for x-ray scattering experiments and the hole concentration dependence of Bragg peak integrated intensity of 3D CDW signal (the colored area is eye guides)

integrated intensity decreases with decreasing hole concentration from 0.12 to 0.07. In the concentration of 0.07, it was not possible to find a CDW peak, even if the superconductivity was completely suppressed. At a slightly increased hole concentration of 0.08, a tiny peak shows up above 15 T, and a sizable intensity is found. These results indicate clearly that the 3D CDW phase terminates at approximately a hole concentration of 0.08 [2].

The present result shows the existence of a quantum critical point (QCP) at approximately 0.08. The end point of the spin density wave phase and the termination point of the field-induced phase transition found in the ultrasound experiment were also approximately 0.08. These evidences establish the existence of a QCP of high-field phase in $\text{YBa}_2\text{Cu}_3\text{O}_x$. Because this QCP is hidden in zero or lower magnetic fields, the high-field ability provides a unique route to access there.

References

- [1] S. Gerber *et al.*, *Science* **357**, 71 (2017).
- [2] H. Jang *et al.*, *Phys. Rev. B* **97**, 224513 (2018).

Keywords: high magnetic field, superconducting, X-ray scattering
 Hiroyuki Nojiri (Magnetism Research Laboratory)
 E-mail: nojiri@imr.tohoku.ac.jp
 URL: <http://www.hfpm.imr.tohoku.ac.jp>

Demonstration of Spin Current Switching

Spin current switching was discovered in Cr_2O_3 , which allows information processing using fully spin-based devices. Our demonstration fills in a missing piece in spintronic devices and is the equivalent of using a transistor to control the flow of electricity.

Spintronics is an emerging field of nanoscale electronics that utilizes not only the charge of the electrons but also the degree of freedom of their spin. In this field, a spin current, a flow of spin-angular momentum, plays an essential role. Owing to the development of spintronics, the detection and generation technologies for the spin current have been well established. However, there is a missing fundamental component in spintronics, namely, a spin-current switch. Here, we demonstrate that a trilayer-film structure consisting of yttrium-iron-garnet YIG ($\text{Y}_3\text{Fe}_5\text{O}_{12}$)/ Cr_2O_3 /Pt operates as a spin-current switch in which the spin-current transmission from YIG to Pt through Cr_2O_3 can be modulated by up to 500% at the antiferromagnetic transition temperature of approximately $T_N = 296$ K for Cr_2O_3 [1].

We fabricated a trilayer film where an antiferromagnetic insulator Cr_2O_3 is sandwiched between a magnetic insulator YIG and a heavy metal Pt film (Fig. 1a). Here, the YIG serves as a spin-current source. By applying a temperature gradient, ∇T , perpendicular to the film planes, the spin Seebeck effect (SSE) [2] generates a spin accumulation at the interface of YIG/ Cr_2O_3 , which drives a spin current (J_s^{in}) into the Cr_2O_3 layer (Fig. 1b). The spin currents transmitted through the Cr_2O_3 layer to the Pt interface (J_s^{out}) are converted into an electric voltage through the inverse spin Hall effect (ISHE).

Figure 2 shows the temperature dependence of the SSE voltage V_{SSE} at $H = 0.1$ T for the YIG/ Cr_2O_3 /Pt trilayer device. Surprisingly, the voltage exhibits an abrupt change of more than 100 times around the Néel temperature of $T_N = 296$ K. The results indicate that the spin-current transmissivity $T_s = J_s^{\text{out}}/J_s^{\text{in}}$ of Cr_2O_3 changes by more than 100 times at approximately T_N . We also found that the spin-current transmissivity T_s of Cr_2O_3 has an anisotropic response to the applied magnetic field H and exhibits a nearly 500% increase under the application of a magnetic field slightly below T_N (see the inset in Fig. 2). These results indicate that the device operates as a spin-current switch when crossing the T_N of Cr_2O_3 or applying a magnetic field. These results are explained through a combination of the anisotropic spin-current transmission of the antiferromagnet and the device

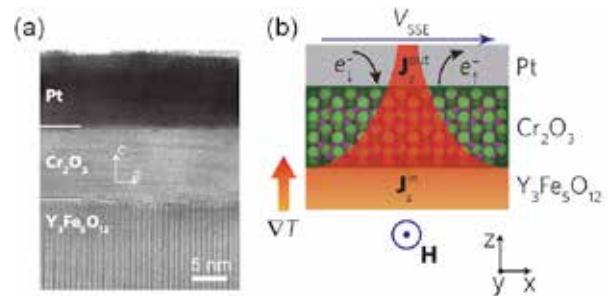


Fig. 1 (a) A cross-sectional TEM image of the YIG/ Cr_2O_3 /Pt trilayer device used in this study. (b) A schematic illustration of the spin-current transmission in YIG/ Cr_2O_3 /Pt induced by the SSE in YIG.

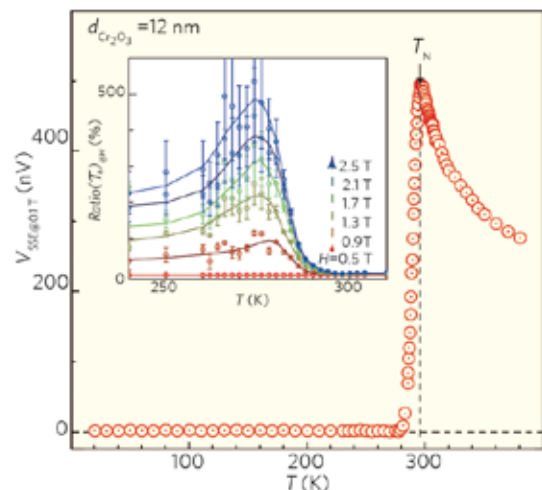


Fig. 2 The temperature dependence of the SSE voltage V_{SSE} at $H = 0.1$ T for the YIG/ Cr_2O_3 /Pt trilayer device with a Cr_2O_3 thickness of 12 nm. The inset shows the temperature dependence of the T_s change ratio, $\text{Ratio}(T_s)@H$, at several H values when the magnetic field H having an out-of-plane component is applied.

geometry, which is correlated with the Néel vector and the anisotropy of Cr_2O_3 [1].

References

- [1] Z. Qiu, D. Hou, J. Barker, K. Yamamoto, O. Gomonay, and E. Saitoh, *Nat. Mater.* **17**, 577 (2018).
- [2] K. Uchida, H. Adachi, T. Kikkawa, A. Kirihara, M. Ishida, S. Yoroza, S. Maekawa, and E. Saitoh, *Proc. IEEE* **104**, 1946 (2016).

Keywords: spintronics, spin current, antiferromagnets

Takashi Kikkawa and Eiji Saitoh (Surface and Interface Research Laboratory)

E-mail: t.kikkawa@imr.tohoku.ac.jp, eizi@imr.tohoku.ac.jp

URL: <http://saitoh.imr.tohoku.ac.jp/>

Taking Aim at the Surface State in Topological Insulator Films

A thin-film fabrication and Fermi-level tuning of a three-dimensional topological insulator (3D-TI) are essential for observing the exotic physical properties originating from Dirac electronic states. In this study, we succeeded in the thin-film growth of a representative 3D-TI Bi_2Se_3 and control of its Fermi level through chemical doping and an electrostatic gating technique. Our achievements will pave the way for an exploration of novel quantum phenomena based on the surface states of 3D-TI.

A three-dimensional topological insulator (3D-TI) (known as a newly discovered class of materials) consists of an insulator in its interior but contains a metallic state at its surfaces (Fig. 1(a)) [1,2]. The metallic surface state hosts a linearly dispersive electronic band, called a Dirac band (green area in Fig. 1(b)). The emergence of exotic physical properties is anticipated in a Dirac-like surface band of 3D-TIs.

To observe the Dirac features from an electrical transport, a tuning of the Fermi-level (E_F) into the bulk band gap is required. However, Bi_2Se_3 , a typical 3D-TI, tends to be an n -type degenerate semiconductor, leaving E_F in the bulk conduction band (gray in Fig. 1(b)). To tackle this issue, we attempted to control E_F in thin films and heterostructures.

A molecular-beam epitaxy (MBE) has been utilized to grow Bi_2Se_3 -based alloy thin films. The $(\text{Bi}_{1-x}\text{Sb}_x)_2\text{Se}_3$ layers were epitaxially grown on a semi-insulating $\text{InP}(111)$ substrate with an isostructural Bi_2Se_3 buffer layer [3]. We observed a clear conversion of the carrier type from an n -type to a p -type by increasing the Sb composition while maintaining the topological nature, which demonstrates the successful tuning of E_F into the surface state.

Aiming at further precise control of E_F , we fabricated a field-effect transistor based on a channel consisting of a $(\text{Bi}_{0.26}\text{Sb}_{0.74})_2\text{Se}_3/\text{Bi}_2\text{Se}_3$ bilayer, as schematically shown in the inset of Fig. 1(c) [4]. The gate-voltage (V_G) dependence of the channel resistance (R_{xx}) exhibits a clear peak (red line), which is absent in a non-doped Bi_2Se_3 layer (black line). Such a marked V_G dependence of R_{xx} is a characteristic of a Dirac electron system, with E_F scanned by V_G across the charge-neutral point.

The developed E_F tuning techniques provide a new arena of Bi_2Se_3 heterostructures for the exploration of exotic phenomena in a Dirac surface state.

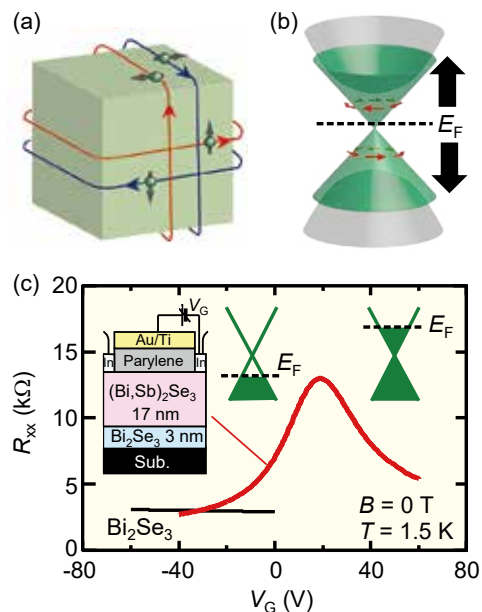


Fig. 1 (a) Schematics of helical surface state of a 3D topological insulator and (b) energy dispersion of the Dirac (green) and bulk (gray) bands. (c) Gate-voltage (V_G) dependence of the sheet resistance (R_{xx}) in field-effect transistors based on non-doped Bi_2Se_3 (black) and $(\text{Bi}_{0.26}\text{Sb}_{0.74})_2\text{Se}_3$ films (red).

References

- [1] X. L. Qi and S. C. Zhang, *Rev. Mod. Phys.* **83**, 1057 (2011).
- [2] Y. Tokura, K. Yasuda, and A. Tsukazaki, *Nature Rev. Phys.* **1**, 126 (2019).
- [3] Y. Satake, J. Shiogai, D. Takane, K. Yamada, K. Fujiwara, S. Souma, T. Sato, T. Takahashi, and A. Tsukazaki, *J. Phys. Condens. Matter* **30**, 085501 (2018).
- [4] Y. Satake, J. Shiogai, K. Fujiwara, and, A. Tsukazaki, *Phys. Rev. B* **98**, 125415 (2018).

Self-Assembled Structure and Related Mesoscopic Two-Dimensional Charge Transport in Conductive Polymer Films

The self-assembled structure and related charge-transport properties in a conductive polymer PEDOT:PSS were revealed by using high-resolution wide-angle X-ray scattering with synchrotron radiation and magnetotransport studies. The results indicate that a mesoscopic two-dimensional coherent transport can be realized owing to the self-assembled laminated structure in a polymer film.

Poly (3,4-ethylenedioxythiophene):poly(styrene sulfonate), abbreviated as PEDOT:PSS, is one of the most commonly utilized conducting polymers in organic electronics. Its electrical conductivity exceeding 1,000 S/cm has been achieved through an improvement of the film fabrication process. Despite such progress, the charge-transport mechanism is still under debate and remains unresolved. The electrical properties of PEDOT:PSS films are strongly related to their complicated macromolecular structures [1], and hence clarification of the correlations between their electrical and structural properties is an active research area in polymer science. We have attempted to reveal this issue through simultaneous structural and transport experiments [2].

The inset in Fig. 1 shows a schematic illustration of a PEDOT:PSS film structure based on grazing-incidence wide-angle X-ray scattering (GIWAXS) experiments conducted using synchrotron radiation light (SPring-8, BL40B2). We investigated that highly conductive PEDOT:PSS films with nearly 1,000 S/cm at room temperature have a nanometer-scale self-assembled laminated structure, which is composed of PEDOT nanocrystals wrapped by insulating sheets consisting of amorphous PSSs. This laminated structure has a characteristic period of ~ 3.0 nm along the vertical direction.

To elucidate the charge-transport mechanism within such a self-assembled structure in detail, we conducted high-field magnetoconductance measurements at up to 15 T [2]. Interestingly, we observed a remarkable positive magnetoconductance at low temperatures, which indicates the existence of the weak localization effects, as shown in Fig. 1. These magnetoconductance curves are quite anisotropic and show good agreement with the theoretical model of a two-dimensional weak localization. The inelastic scattering length obtained, i.e., the average distance a charge travels between inelastic collisions, is approximately 3.5 nm at 100 K and

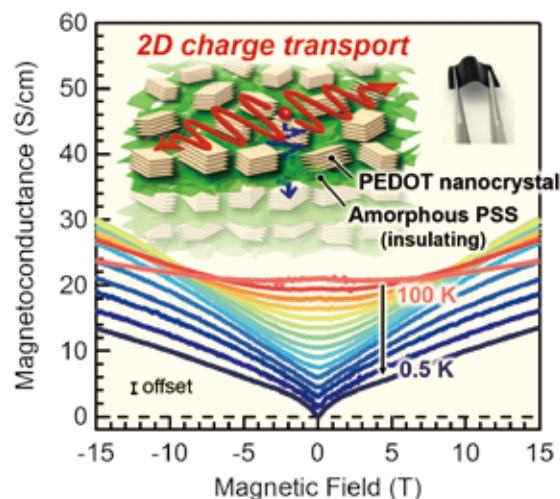


Fig. 1 Magnetoconductance curves at various temperatures. The inset shows a schematic of the film structure based on X-ray scattering experiments conducted at SPring-8.

increases with a decrease in temperature. Importantly, if a charge is confined within a layer thinner than the inelastic scattering length, the charge transport is regarded as a two-dimensional system from the viewpoint of not only the absolute conductivity but also the electronic coherence. This condition can be satisfied at below 100 K; that is, the results strongly suggest that the motion of electrons is confined within the laminated structure at low temperatures. The results indicate that a two-dimensional coherent transport can be realized even in polymer films fabricated using a simple drop-casting method for commonly used materials.

References

- [1] T. Takano, H. Masunaga, A. Fujiwara, H. Okuzaki, and T. Sasaki, *Macromolecules* **45**, 3859 (2012).
- [2] Y. Honma, K. Itoh, H. Masunaga, A. Fujiwara, T. Nishizaki, S. Iguchi, and T. Sasaki, *Adv. Electron. Mater.* **4**, 1700490 (2018).

Keywords: polymer, GIWAXS, magnetoconductance

Takahiko Sasaki (Low Temperature Condensed State Physics Research Laboratory)

E-mail: takahiko@imr.tohoku.ac.jp

URL: <http://cond-phys.imr.tohoku.ac.jp/>

Reduction Annealing Effects on Electronic States in T'-Structured Cuprates Studied by X-Ray Absorption Spectroscopy

Both cation-site substitution and post annealing in a reducing atmosphere are key treatments for the emergence of superconductivity in T'-structured cuprates. To reveal the effects of reduction annealing on the electronic states, we conducted a Cu K-edge X-ray absorption spectroscopy study on superconducting and non-superconducting T'-structured $\text{Pr}_{2-x}\text{Ce}_x\text{CuO}_{4+\alpha-\delta}$ (PCCO) samples. An X-ray absorption near-edge structure (XANES) shows a clear increase in the number of electron carriers in the annealed samples. Based on this result, we suggest that the annealing effect on PCCO is qualitatively equivalent to that of the cation, *e.g.*, Ce, substitution. Furthermore, an analysis of the XANES spectra indicates that, in addition to electrons, hole carriers possibly exist in heavily doped $\text{Pr}_{2-x}\text{Ce}_x\text{CuO}_{4+\alpha-\delta}$ samples.

$\text{RE}_{2-x}\text{Ce}_x\text{CuO}_4$ ($\text{RE} = \text{Pr}, \text{Nd}, \text{Sm}, \text{Eu}$) with a T'-type structure is a family of high-temperature superconductors. In this system, both Ce substitution and reduction annealing are needed for an emergence of the bulk superconductivity. Angle-resolved photoemission spectroscopy studies have recently revealed that the number of electrons per Cu ion increases through an appropriate heat treatment in a reducing atmosphere [1]. This result suggests that the carrier concentration is strongly affected by the non-stoichiometry of oxygen. However, the relationship between the concentration of oxygen vacancies, δ , and the carrier number has yet to be clarified. Therefore, clarifying the effects of annealing in a reducing atmosphere is an important issue. In this study, we succeeded in estimating the carrier concentration in PCCO through Cu K-edge XANES measurements [2].

Figure 1 shows Cu K-edge XANES spectra for as-sintered PCCO with $x = 0 - 0.2$. The XANES spectra vary with the Ce substitution. A peak at 8980 eV corresponds to the $1s-4p\pi$ dipole transitions of Cu^+ ions. The peak intensity gradually increases with an increase in x , indicating an increase in the number of Cu^+ ions. Because the number of Cu^+ ions is proportional to the number of electron carriers, we can evaluate the effective variation of the carrier concentration by analyzing the change in intensity at 8980 eV. In the as-sintered PCCO system, we found that the number of electrons evaluated, n_{Ce} , is proportional to x . In contrast, the XANES intensity at 8980 eV shows a strange variation as a function of oxygen loss δ , as displayed in Fig. 2. This means that the number of doped electrons, n_{AN} , in the annealed PCCO system is not equal to 2δ . Considering the charge neutrality, a deviation of n_{AN} from 2δ suggests that two types of carriers are doped in the system.

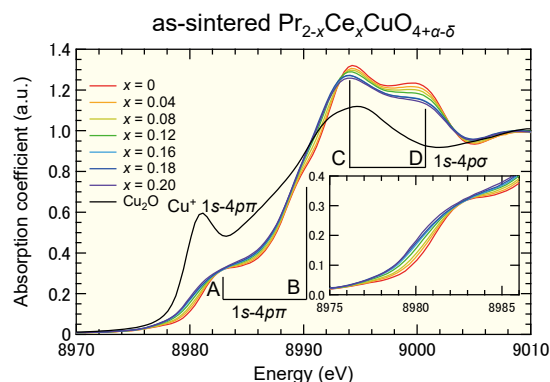


Fig. 1 Cu K-edge absorption near-edge spectra for the as-sintered $\text{Pr}_{2-x}\text{Ce}_x\text{CuO}_{4+\alpha-\delta}$. The spectrum of Cu_2O is shown as a reference.

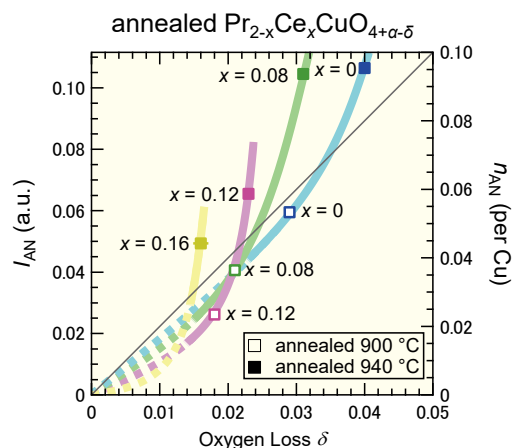


Fig. 2 Variation of intensity of the $\text{Cu}^+ 1s-4p\pi$ dipole transition as a function of δ . The right axis shows the evaluated number of electrons per Cu ion. The solid line represents a relation of $n_{\text{AN}} = 2\delta$, which is expected from the charge neutrality.

References

- [1] D. Song *et al.*, Phys. Rev. Lett. **118**, 137001 (2017).
- [2] S. Asano *et al.*, J. Phys. Soc. Jpn. **87**, 094710 (2018).

Keywords: electronic structure, superconducting, XAFS

Masaki Fujita (Quantum Beam Materials Physics Research Laboratory)

E-mail: fujita@imr.tohoku.ac.jp

URL: <http://qblab.imr.tohoku.ac.jp/index.html>

Surface Acoustic Wave on Multiferroics

Multiferroics are functional materials having both ferroelectricity and magnetism. The interplay between them gives rise to unique material functionalities such as a magneto-electric effect. Herein, we demonstrated the magnetic field dependent surface acoustic wave (SAW) propagation on the multiferroics BiFeO₃ and CuB₂O₄. This phenomenon is induced through an interplay between magnetism and piezoelectricity.

A surface acoustic wave (SAW) is an elastic wave propagating on the surface of a material. The excitation and detection of a SAW can be achieved using an interdigital transducer (IDT) on a piezoelectric material. As shown in Fig. 1(a), the IDT is composed of a pair of comb-like electrodes. Only when the SAW wavelength coincides with twice the sum of the finger width and space, the IDT can operate as a SAW electromagnetic wave transducer, and the electromagnetic signal can transmit from one IDT to another through SAW propagation. In this way, a device composed of two IDTs on a piezoelectric substrate operates as a band pass filter. A SAW filter can be considerably miniaturized, and thus such band-pass filters are widely applied in electronics used in small spaces. If the substrate of a SAW band-pass filter device is replaced with a multiferroic material, the transmission strength and frequency can be controlled using an external magnetic field. The novel functionality of a field tunable band-pass filter seems to be useful for future high-frequency electronics.

We observed SAW propagation on a multiferroic BiFeO₃. Figure 1(b) shows the transmittance between the IDTs for the BiFeO₃ SAW device. A sharp peak is discerned at approximately 50 MHz. This peak is induced by SAW propagation between the IDTs. The broad peak at approximately 150 MHz is the remnant of the third harmonics. To study the effects of multiferroicity on the SAW propagation, we investigated the magnetic field variation of SAW propagation. Figure 1(c) shows the transmission change as a function of the magnitude and angle of the magnetic field for the BiFeO₃ SAW device. The SAW transmission becomes dependent on the angle of the magnetic field in a high field region. The magnetic field dependence can be explained based on the magnetoelastic coupling in a helimagnetic state, as detailed in [1]. We also observed SAW propagation in other multiferroic CuB₂O₄ [2]. We fabricated the IDTs using a finger period of 800 nm. As a result, SAW excitation reaches as high as 3 GHz and is coupled to the

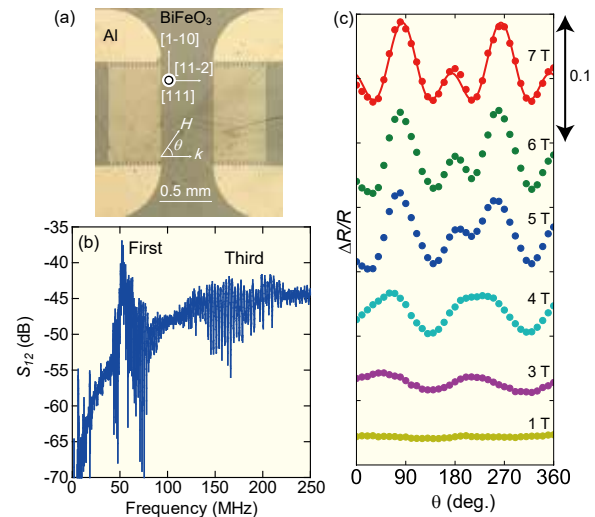


Fig.1 (a) Optical microscope image of BiFeO₃ device. The two IDT electrodes are deposited on a BiFeO₃ single crystal. (b) Transmission spectrum between two IDTs. The sharp peak at approximately 50 MHz is induced through SAW propagation. (c) The relative change of the SAW propagation amplitude as a function of the angle of the magnetic field at various magnitudes.

antiferromagnetic magnons. Magnetic field modulation through coupling is also observed.

References

- [1] Y. Ishii, R. Sasaki, Y. Nii, T. Ito, and Y. Onose, Phys. Rev. Applied **9**, 034034 (2018).
- [2] R. Sasaki, Y. Nii, and Y. Onose, Phys. Rev. B **99**, 014418 (2019).

Keywords: multi-ferroics, piezoelectric, devices

Yoshinori Onose (Quantum Functional Materials Physics Research Laboratory)

E-mail: onose@imr.tohoku.ac.jp

URL: <http://onoselab.imr.tohoku.ac.jp/index.html>

Hydrogen Behavior in $\text{Al}_2\text{O}_3/\text{Hf}_x\text{Si}_{1-x}\text{O}_2/\text{SiO}_2$ Gate Dielectric Stacks in Memory Device Structures Analyzed by Atom Probe Tomography

Hydrogen (H) plays an important role in determining the reliability and performance of high- k dielectric electronic memory devices. To understand the H behavior, deuterium (D), an isotope of H, was introduced into a poly-Si cap of $\text{Al}_2\text{O}_3/\text{Hf}_x\text{Si}_{1-x}\text{O}_2/\text{SiO}_2$ high- k stacks. Our results obtained through atom probe tomography demonstrated that Al_2O_3 blocks the H atoms at the surface, preventing them from diffusing into the high- k dielectrics during the H_2 annealing process.

Aluminum oxide (Al_2O_3) can be used in combination with high-permittivity (high- k) materials based on hafnium oxide (HfO_2) as gate dielectrics in non-volatile memory devices. In general, hydrogen (H_2) sintering, *i.e.*, annealing in H_2 ambient in the back-end-of-line (BEOL) process, is required to acquire a high-quality interface. However, excess H_2 diffusion into the substrate or dielectric region can affect the device performance. The exact mechanism or trapping capability in metal oxides has yet to be properly investigated. It has been suggested that control of the H species diffusion should be taken into consideration during the process optimization from the viewpoint of reliability.

Laser-assisted atom probe tomography (APT) has been proven useful to obtain three-dimensional atom maps of semiconductor materials [1, 2]. As with other conventional techniques, observation and a quantitative analysis of H remain difficult in APT owing to the absorption of H atoms from residual gas in the analysis chamber as an artifact during the measurement. Therefore, we implanted deuterium (D), an isotope of H, into the samples at a high dose to distinguish it from H in the residual gas. Here, we report an APT study of ion-implanted D behavior in $\text{Al}_2\text{O}_3/\text{Hf}_x\text{Si}_{1-x}\text{O}_2/\text{SiO}_2$ (AHO) high- k stacks with poly-Si cap, as shown in Fig. 1(a), under different annealing temperatures [3].

Figure 1(b) shows atom maps of elements containing the AHO as-implanted regions, annealed at 600 or 900 K for 10 min. Peak 2 (p2) of the mass-to-charge state ratio obtained from the APT mass spectrum is defined as D. In the sample annealed at 900 K for 10 min, a clear segregation of p2 was observed (Fig. 1(c)), meaning that the D atoms diffused toward the AHO region and became trapped at the poly-Si/ Al_2O_3 interface. This indicates that the use of Al_2O_3 can effectively prevent H diffusion at the interface during the BEOL process.

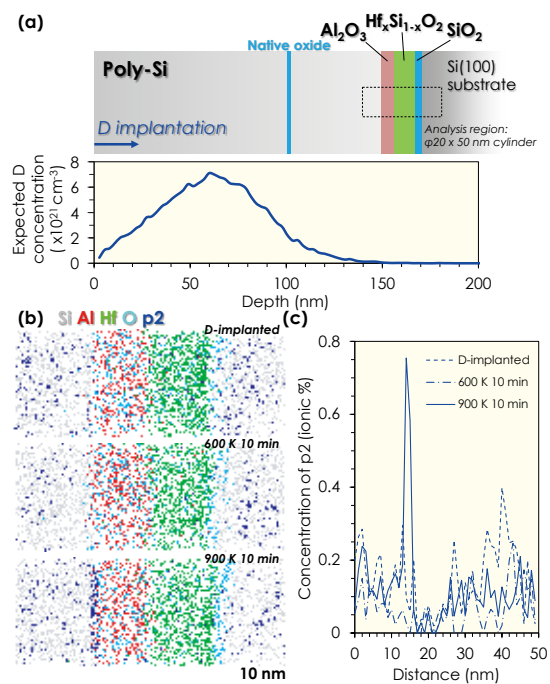


Fig. 1 (a) Schematic illustration of the sample structure and the expected D concentration on the basis of simulation. (b) Atom maps and (c) concentration profiles of peak 2 in a $\phi 20 \times 50$ nm cylinder containing the AHO regions processed under different conditions.

The current study provides an example of the H behavior in semiconductors using APT.

References

- [1] A. D. Giddings, S. Koelling, Y. Shimizu, R. Estivill, K. Inoue, W. Vandervorst, and W. K. Yeoh, *Scripta Mater.* **148**, 82 (2018).
- [2] Y. Tu, Y. Shimizu, Y. Kunimune, Y. Shimada, T. Katayama, T. Ide, M. Inoue, F. Yano, K. Inoue, and Y. Nagai, *J. Appl. Phys.* **124**, 155702 (2018).
- [3] Y. Tu, B. Han, Y. Shimizu, Y. Kunimune, Y. Shimada, T. Katayama, T. Ide, M. Inoue, F. Yano, K. Inoue, and Y. Nagai, *Appl. Phys. Lett.* **112**, 032902 (2018).

Keywords: atom probe tomography, hydrogen implantation, electronic material

Yasuo Shimizu, Koji Inoue, Kazuaki Nagumo, and Yasuyoshi Nagai (Irradiation Effects in Nuclear and Their Related Materials Research Laboratory)

E-mail: yshimizu@imr.tohoku.ac.jp

URL: <http://wani.imr.tohoku.ac.jp/index.html>

History of Research on Nitride Semiconductors and Recent Results

Since the proposal of the material InGaAlN for blue-emitting diodes in 1986 and the success in the epitaxial growth of single-crystalline InGaN as a blue-light emitting material in 1989 by Nippon Telegraph & Telephone, research has continued on the new field of nitride semiconductors as materials and their device applications to realize a sustainable society, in the Department of Electronic Materials of the Institute for Materials Research for more than 14 years till the retirement at the end of March 2019. The main themes and the recent results are shown below.

Historical Research

1. Crystalline polarity originated from wurtzite N-Polarity GaN on Sapphire Substrate Grown by MOVPE

Ga-polar GaN used in blue LEDs was used on (0001) sapphire by metalorganic vapor-phase epitaxy (MOVPE). N-polar GaN with the same characteristics as G-polar one was successfully grown. This result gives the flexibility for device design, because the direction of the spontaneous polarization depends on the polarity.

2. High-quality InN epitaxial growth

InN is the last emerging material among nitride semiconductor InGaAlN. For a long time, a single crystalline InN has not been obtained, because of the extremely high equilibrium vapor pressure of nitrogen. Single-crystalline InN was obtained by using the N-polar growth and the pressurized-reactor MOVPE system developed in-house. This result can extend the emitting wavelength region of InGaAlN to the infrared.

3. Measurement of internal electric fields

A nitride semiconductor has a strong polarization-induced internal electric field, which affects the device performance. The direct measurement of the internal electric field was done successfully.

4. Observation of dislocation in GaN

A three-dimensional imaging of threading dislocations in GaN was demonstrated by using multiphoton-excitation photoluminescence [1]. This method can be considered a novel method for characterizing defects in GaN films without any destructive preparations.

Recent Result

An N-polar high-electron-mobility transistor (HEMT) consists of a structure advantageous to high-performance device characteristics for a short length of a gate, because the channel at the top surface makes the carrier confinement high. Because the N-polar growth is said to be difficult

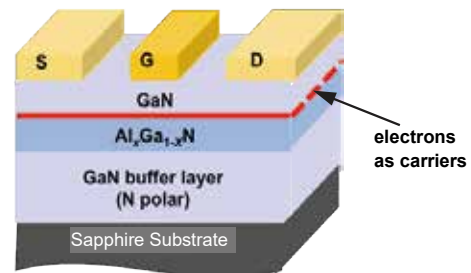


Fig. 1 Structure of N-polar HEMT

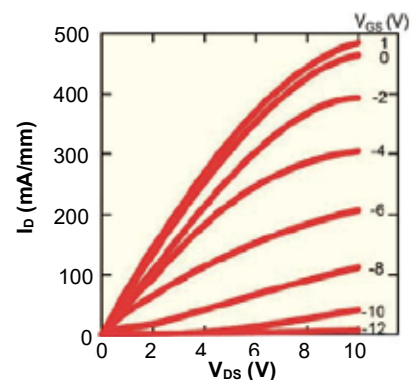


Fig. 2 Source-drain voltage vs. drain current

from compared with the Ga-polar one, there are not so many reports on these devices. By optimizing the growth conditions, including the off-cut angle of a sapphire substrate, it was possible to obtain the HEMT structure without hillocks and step-bunching. A HEMT was also fabricated, and the operation of field-effect transistors was confirmed. Suppressing the step-bunching by using a small off-cut angle made it possible to obtain the device characteristics with less anisotropy, compared with the previously reported N-polar HEMT [2]. This result is very important for the device design.

References

- [1] T. Tanikawa, K. Ohnishi, M. Kanoh, T. Mukai, and T. Matsuoka, *Appl. Phys. Express* **11**, 031004 (2018).
- [2] K. Prasertsuk, T. Tanikawa, T. Kimura, S. Kuboya, T. Suemitsu, and T. Matsuoka, *Appl. Phys. Express* **11**, 015503 (2018).

Keywords: nitride semiconductors, GaN, epitaxial growth

Takashi Matsuoka (Physics of Electronic Materials Research Laboratory)

E-mail: matsuoka@imr.tohoku.ac.jp

URL: <http://www.matsuoka-lab.imr.tohoku.ac.jp>

Gas-Responsive Porous Magnet Distinguishes the Electron Spin of Molecular Oxygen

Gas-sensing materials are of increasing societal importance, although differentiating between similarly sized gases such as N₂ and O₂ remains a significant challenge. Herein, we report a porous ferrimagnet that distinguishes diamagnetic N₂ and CO₂ gases from paramagnetic O₂ gas.

Studies on molecular porous materials, so-called metal-organic frameworks (MOFs), have attracted significant attention, in which the design of gas-responsive magnetic materials is a critical issue. We reported a compound responsive to an organic-solvent vapor showing a drastic change in the magnetic ordering temperature (T_c) [1]. Nevertheless, a lack of candidates in magnetic materials responsive to common gases such as N₂, CO₂, and O₂ is rather curious. Herein, we report the first porous magnetic material whose magnetic phases are switchable through gas adsorption/desorption, i.e., a *gas-responsive porous magnet* [2].

A porous ferrimagnet with $T_c = 76$ K, which is composed of a 2:1 assembly of a paddlewheel-type diruthenium(II,II) complex and a derivative of 7,7,8,8-tetracyano-*p*-quinodimethane (TCNQ), exhibits reversible gas sorption properties for N₂, CO₂, and O₂, accompanying a structural modulation. Whereas the uptake of N₂ and CO₂, despite their diamagnetic characteristics, leads to an increase of T_c to 88 K and 92 K, respectively, the uptake of O₂ reveals a continuous phase change from a ferrimagnet involving the increase of T_c at low gas pressures to an antiferromagnet at high gas pressures (Fig. 1a). The observed increase of T_c through a gas insertion is explained by a gas-induced structural modification, i.e., the modification of magnetic pathways, whereas the insertion of paramagnetic O₂ induces a magnetic phase switch between a ferrimagnet and an antiferromagnet based on the formation of new magnetic pathways which O₂ itself mediates (Fig. 1b). The magnetic switching between a ferrimagnet and an antiferromagnet is quite fast and reversible (Fig. 1c). This chameleonic material, the first with switchable magnetism that can discriminate between similarly sized N₂ and O₂ gases, provides a wide scope of new gas-responsive porous magnets.

References

[1] J. Zhang, W. Kosaka, K. Sugimoto, and H. Miyasaka, *J. Am. Chem. Soc.* **140**, 5644 (2018).

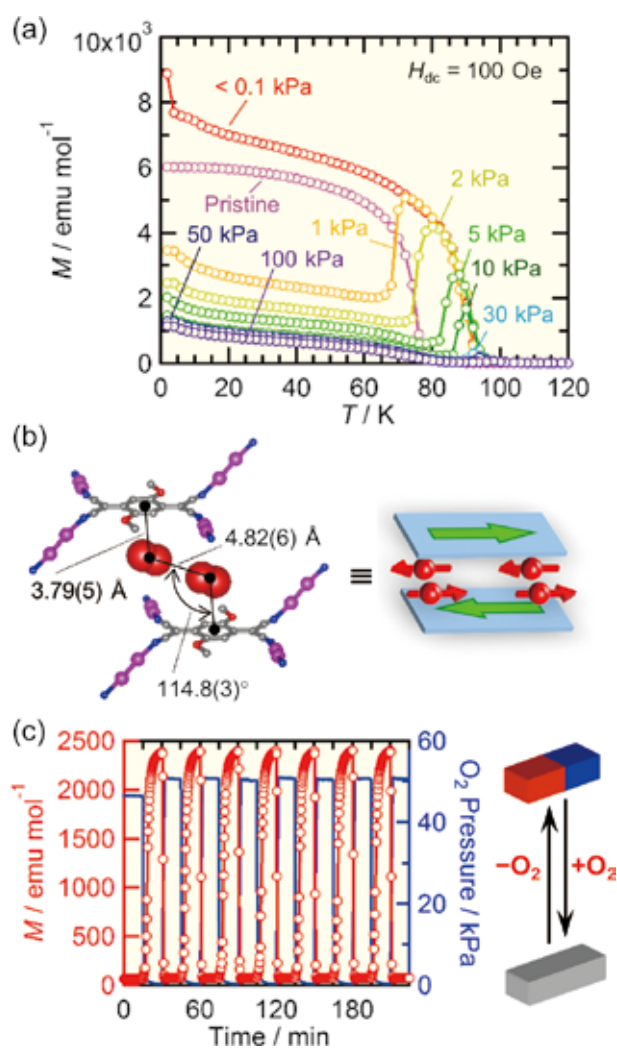


Fig. 1 (a) Temperature dependence of magnetization under O₂. (b) Crystal structure of O₂-adsorbed phase focused on adsorbed O₂ and scheme of the magnetic moment alignment. (c) ON/OFF switching of magnetization through O₂ desorption/adsorption at 85 K and $H_{dc} = 100$ Oe.

[2] W. Kosaka, Z. Liu, J. Zhang, Y. Sato, A. Hori, R. Matsuda, S. Kitagawa, and H. Miyasaka, *Nat. Commun.* **9**, 5420 (2018).

Keywords: ferromagnetic, antiferromagnetic, porosity

Wataru Kosaka and Hitoshi Miyasaka (Solid-State Metal-Complex Chemistry Research Laboratory)

E-mail: w-kosaka@imr.tohoku.ac.jp (W. K.); miyasaka@imr.tohoku.ac.jp (H. M.)

URL: <http://www.miyasaka-lab.imr.tohoku.ac.jp/cn5/HOME-Eng.html>

Crystallization “Manipulated” by Plasmonic Optical Tweezers

Control of the crystallization by an external field impacts the creation of functional crystalline materials. Herein, we show that plasmonic optical tweezers, the trapping force of which relies on an electrical field gradient generated by the plasmonic near-field within the proximity of a metal nanostructure, can reversibly “manipulate” the crystallization/dissolution of a dielectric material in a solution.

Complete spatiotemporal control of crystallization through an external field impacts not only the technology used to create functional crystalline materials but also the exploration during the early stage of dynamics of crystallization hidden in the stochastic nature of nucleation. Tremendous efforts have been recently devoted to the control of crystallization by trapping dielectric molecular clusters in a solution using optical tweezers, the trapping force of which relies on the gradient of the electrical field generated by focusing a laser with an optical lens [1]. This strategy has induced a forced crystallization even from an unsaturated solution. However, light focusing applied to enhance the trapping force is intrinsically limited by the diffraction limit of the optical lens, hindering an increase in the controllability. To overcome this limitation, in the present study, we applied a near-field confined beyond the diffraction limit generated by the surface plasmon resonance (SPR) on a metal nanostructure.

A Au gammadion nanolattice was fabricated on a cover glass using electron beam lithography (Fig. 1a). An aqueous solution of acetaminophen saturated at room temperature (24 °C) was dropped on the nanolattice, and a thin layer solution was then formed by the capillarity. Continuous-wave circularly polarized laser ($\lambda = 1,064 \text{ nm}$, $6.4 \times 10^9 \text{ W/m}^2$) was focused on the nanolattice to excite the SPR through an objective lens on an optical microscope while conducting *in-situ* observations.

The plasmon excitation allowed molecules to crystallize in an annular distribution with a size of 1,000 nm for each crystal (Fig. 1b). A numerical analysis of the electromagnetic field and temperature distribution measurement indicate that the annular pattern is probably a consequence of the balance between the electrical field gradient force toward the focal spot and the opposite thermophoretic force from plasmonic heating [2, 3]. The position of the pattern was found to be manipulatable through a coupled dissolution/precipitation process by moving the position of the focal spot. The stopping of the plasmon excitation resulted in a disappearance of the crystals through an unprecedented two-step

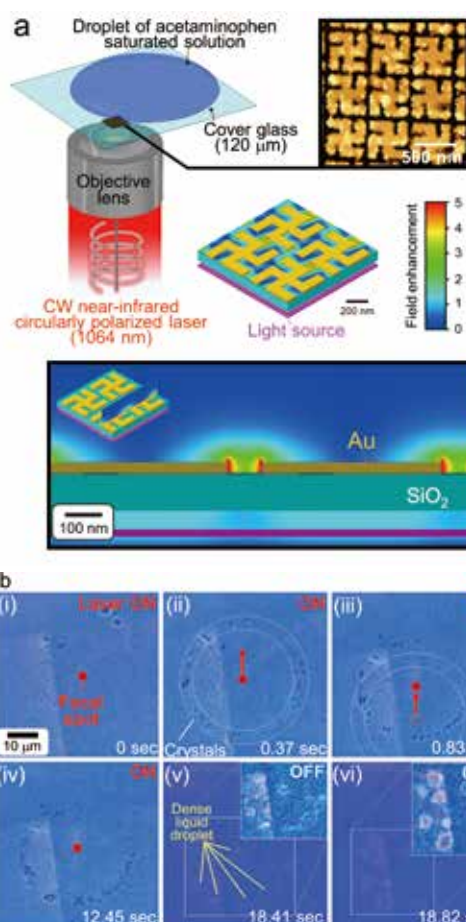


Fig. 1 (a) Experimental setup and electrical field distribution analyzed using FDTD method. (b) *In-situ* observation of crystallization dynamics.

dissolution process, and the transformation into liquid droplets followed through relaxation by diffusion. Our results indicate that plasmonic optical tweezers can “manipulate” the crystallization precisely, and lead to unprecedented phenomena.

References

- [1] K. Yuyama, M. J. Islam, K. Takahashi, T. Nakamura, and V. Biju, *Angew. Chem. Int. Ed.* **130**, 13612 (2018).
- [2] H. Niinomi, T. Sugiyama, S. Uda, M. Tagawa, T. Ujihara, K. Miyamoto, and T. Omatsu, *Cryst. Growth Des.* **19**, 529 (2019).
- [3] T. Shoji and Y. Tsuboi, *J. Phys. Chem. Lett.* **17**, 2957 (2014).

Keywords: nucleation & growth, metal, nanostructure
 Hiromasa Niinomi (Crystal Chemistry Research Laboratory)
 E-mail: h.niinomi@imr.tohoku.ac.jp
 URL: <http://www.uda-lab.imr.tohoku.ac.jp>

Splitting Fermi Surfaces in Non-Centrosymmetric Heavy Fermion Compound $U_3Ni_3Sn_4$

We investigated the Fermi surface properties on non-centrosymmetric heavy fermion compounds $U_3Ni_3Sn_4$ based on de Haas-van Alphen experiments using a high-quality single crystal. Many closed Fermi surfaces with heavy effective masses of up to 35 m_0 were clearly detected. Compared to the LDA band structure calculations, it was determined that they originate from the splitting band owing to an antisymmetric spin-orbit coupling. To the best of our knowledge, the splitting Fermi surface from the non-centrosymmetric nature of 5f-electron systems was detected experimentally for the first time.

Non-centrosymmetric compounds have attracted significant attention owing to their anomalous behaviors such as unconventional parity-mixing superconductivity, magnetic skyrmion, multipole orders, and chiral fermiology. Spin-orbit coupling plays an important role in these compounds. Actinide compounds are particularly important targets in this context, because 5f electrons of actinide elements have a large spin-orbit coupling and the electron correlations are strong.

We grew single crystals of a non-centrosymmetric compound, $U_3Ni_3Sn_4$, using the Bridgman method and measured them through de Haas-van Alphen (dHvA) experiments [1]. The residual resistivity ratio (RRR) is 300, indicating a very high quality of the obtained single crystals. $U_3Ni_3Sn_4$ is a paramagnet with a cubic structure (space group: #220, $I\bar{4}3d$). A large Sommerfeld coefficient shows a heavy electronic state, and it is therefore believed that $U_3Ni_3Sn_4$ is located at the verge of the antiferromagnetic quantum critical point.

Figure 1 shows typical dHvA oscillations and the corresponding FFT spectrum. Many fundamental FFT peaks were detected, indicating many Fermi surfaces. The angular dependence of the dHvA frequencies is in good agreement with the results of the LDA band structure calculations. It was found that most of the Fermi surfaces are spherical in shape, derived from 12 bands crossing the Fermi energy. In Fig. 1, the calculated Fermi surfaces for branches β and β' are also shown. The bands are split owing to the antisymmetric spin-orbit coupling, and the splitting energy is estimated to be 20–100 K. The relatively small splitting energy is most likely due to the large effective mass.

This work was conducted in collaboration with A. Maurya, H. Harima, A. Nakamura, Y. Shimizu, Y. Homma, D.X. Li, F. Honda, and Y. J. Sato.

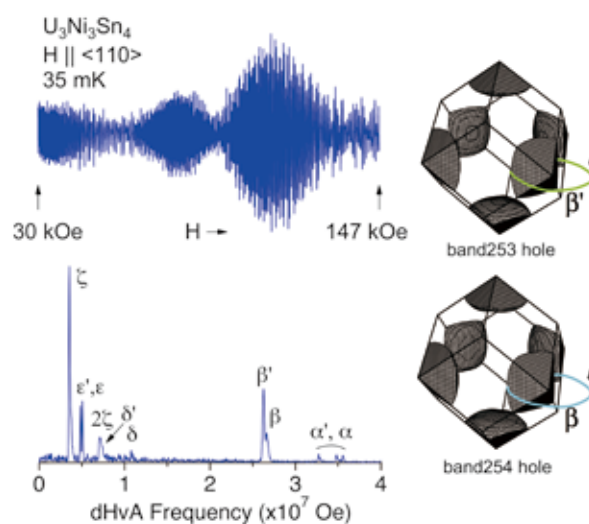


Fig. 1 Typical dHvA oscillations and the corresponding FFT spectrum in a non-centrosymmetric heavy fermion compound, $U_3Ni_3Sn_4$. The calculated splitting Fermi surfaces (branches β and β') due to the antisymmetric spin-orbit coupling are shown on the left-hand side.

References

- [1] A. Maurya, H. Harima, A. Nakamura, Y. Shimizu, Y. Homma, D. X. Li, F. Honda, Y. J. Sato and D. Aoki: J. Phys. Soc. Jpn. **87**, 044703 (2018).

Formation of ZrO₂-Based Ferroelectric Thin Films

Ferroelectricity in epitaxially grown Fe-doped ZrO₂ thin films has been demonstrated. The structures of the 30-nm-thick $x\text{Fe}_2\text{O}_3\text{-(1-x)ZrO}_2$ thin films ($x = 0, 0.03, 0.05,$ and 0.07 , nominal composition) have been examined by X-ray diffraction and scanning transmission electron microscopy, revealing that the monoclinic phase (space group: $P2_1/c$) dominates for $x = 0$, while the films containing Fe exhibit multidomain structures consisting of the monoclinic and orthorhombic phases.

Ferroelectric thin oxide films have been extensively studied as a key material in electronic applications, including nonvolatile memories and low-power transistors. Among them, hafnia (HfO₂)- and zirconia (ZrO₂)-based thin films, which are environmentally friendly and thermodynamically compatible with Si substrates, have recently attracted much attention since the discovery of ferroelectricity in a Si-doped HfO₂ thin film. The dielectric properties of these oxide films are directly related to their crystal structures, and the basic phase transition scheme from high to low temperatures is cubic (*c*), tetragonal (*t*), and monoclinic (*m*). The *m*-phase ($a = 0.515, b = 0.520,$ and $c = 0.532$ nm, $\beta = 99.25^\circ$) is nonpolar and exhibits a simple dielectric behavior, while the emergence of ferroelectricity is ascribed to the polar orthorhombic phase (*o*, space group: $Pbc2_1, a = 0.507, b = 0.526,$ and $c = 0.508$ nm), and much effort has been devoted to the stabilization of the polar phase.

In this study, epitaxial ZrO₂ thin films have been formed on (100)YSZ and (100)ITO/(100)YSZ substrates (YSZ: yttria stabilized zirconia, ITO: indium tin oxide) by sputtering and postannealing. [1, 2] The sputtering targets were prepared by pressing the mixture of Fe₂O₃ and ZrO₂ powders. The crystal structure was investigated by using an X-ray diffractometer. The microstructure was observed by high-angle annular dark-field scanning transmission electron microscopy (HAADF-STEM) operating at 200 kV, with the convergent semiangle (α) and acceptance semiangle of the HAADF detector ($\beta_{\text{in}}\text{-}\beta_{\text{out}}$) set to 20 and 90-175 mrad, respectively.

Figure 1(a) shows cross-sectional HAADF-STEM images of 0.03Fe₂O₃-0.97ZrO₂ thin films, deposited on the (100) YSZ substrates. Bright spots indicate heavy atoms, *i.e.*, cations. As seen, the films are composed with the regions having different crystallographic orientation, or domains. As seen, no misfit dislocation has been observed at the interface. That is, the interface is coherent. Yet, the dark contrast suggests the presence of coherent

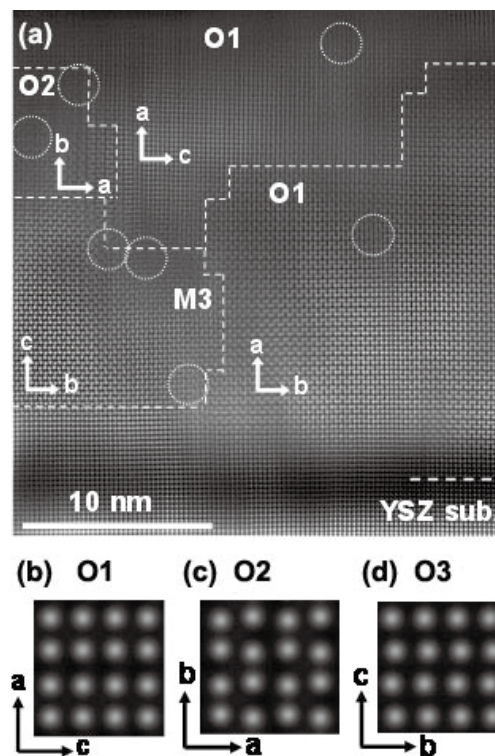


Fig. 1 (a) Cross-sectional HAADF-STEM images of the 0.03Fe₂O₃-0.97ZrO₂ thin films on YSZ substrates viewed along the 100 axis of the substrate, and (b), (c), and (d) simulated HAADF-STEM images of the *o*-phase ($Pbc2_1$) for O1, O2, and O3 domains, respectively

strain within the film — especially, near the substrate. A comparison of the observed images with simulated ones, as in Figs. 1(b)-(d), reveals that, inside the film, *m*- and *o*-phases coexist, as indicated by M3, O1, and O2, thereby forming a multidomain structure. The contrasts in the vicinities of boundaries of these domains are generally dark, indicating the presence of strain fields.

References

- [1] S. Choi, T. Shiraishi, T. Kiguchi, T. Shimizu, H. Funakubo, and T. J. Konno, *Appl. Phys. Lett.* **113**, 262903 (2018).
- [2] T. Shiraishi, S. Choi, T. Kiguchi, T. Shimizu, H. Funakubo, and T. J. Konno, *Jpn. J. Appl. Phys.* **57**, 11UF02 (2018).

Keywords: dielectric, oxide, thin films

Toyohiko J. Konno (Materials Science of Non-Stoichiometric Compounds Research Laboratory)

E-mail: tjkonno@imr.tohoku.ac.jp

URL: <http://konno-lab.imr.tohoku.ac.jp/>

Research Centers

IMR KINKEN Research Highlights 2019



Actinide Oxide Ion Formation in Collision/Reaction Cell of ICP-MS/MS

International Research Center for Nuclear Materials Science

Actinide oxide ion formations in collision/reaction cells of ICP-MS/MS were investigated to explore the possibility of an isobaric discrimination for actinide analyses. We found that the dominant ions are oxide ions, and the ratio of monoxide ion/dioxide ions increases with the atomic number under the same oxygen gas flow rate. The percentages of actinide ions and oxide ions depend on the oxygen gas flow rate, and the number of oxygen ions attached to actinides increases with the oxygen gas flow rate.

The importance of a quantitative actinide and isotope ratio analyses has increased in the nuclear and radioanalytical fields, namely, radio waste management, nuclear forensics, and safeguards. For actinide analyses, α -spectrometry and thermal ionization mass spectrometry (TIMS) have been used. Although these methods have high accuracy and high precision, the measurement time is quite long, and pretreatments are time-consuming. An inductively-coupled plasma mass spectrometer (ICP-MS) has recently come to be used in actinide analyses owing to a short measurement time. From the viewpoint of an accurate and precise actinide analysis, isobaric interferences are a critical issue because actinides have many isotopes, such as ^{241}Pu and ^{241}Am . The mass shift when using molecular ion formations in a collision/reaction cell of ICP-MS is one method with the potential of an isobaric discrimination. Thus, we studied the oxide molecular ion formations of actinides using oxygen gas [1]. A quadrupole type ICP-MS/MS (Agilent 8900), which has two MSs and one collision/reaction cell between them, was used in the present study. The ions with a mass equivalent to each objective actinide nuclide (M) were allowed through the first MS, and the detected ions through the second mass after the reaction with oxygen gas were M^+ , M^{16}O^+ , and $\text{M}^{16}\text{O}_2^+$. The effect of the oxygen flow rate on the oxide ion formation is shown in Fig. 1. The mass shift of $\text{M}^+ \rightarrow \text{MO}^+ \rightarrow \text{MO}_2^+$ with an increase in the oxygen flow rate was confirmed for all actinides, and this shift in actinides with a lower atomic number occurs at a lower oxygen flow rate. It was also confirmed that the oxide ion formation behaviors of the lighter and heavier actinides on the oxygen flow rate are also substantially different. The difference in molecular ion formations among the actinides can be explained based on the electron configuration

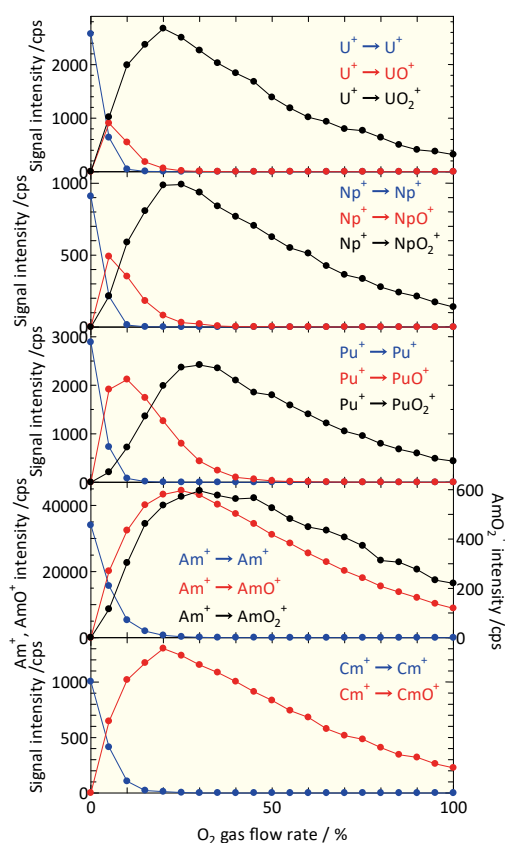


Fig. 1 Oxygen gas flow rate effect on intensities of detected ion species. 100% of flow rate is defined as 1.5 mL/min in nitrogen gas flow.

related to the 5f-electron orbital. From the results obtained, we found the feasibility of an isobaric discrimination through a comparison of the yield using different oxygen gas flow rates.

References

- [1] T. Suzuki, T. Yamamura, C. Abe, K. Konashi, and Y. Shikamori, *J. Radioanal. Nucl. Chem.* **318**, 221 (2018).

Keywords: actinide, mass spectrometry

Tatsuya Suzuki (Corresponding Author, Nagaoka University of Technology)

E-mail: tasuzuki@vos.nagaokaut.ac.jp

Nagai Yasuyoshi (Head of International Research Center for Nuclear Materials Science)

E-mail: nagai@imr.tohoku.ac.jp

URL: <http://www.imr-oarai.jp/>

Contribution of Irradiation-Induced Small Dislocation Loops to Hardening Mechanism of Nuclear Reactor Pressure Vessel Steels Identified by Electron Microscopy

International Research Center for Nuclear Materials Science

The number density and size distribution of dislocation loops in surveillance test specimens of a European pressurized water reactor were systematically evaluated using weak-beam scanning transmission electron microscopy, and their contributions to hardening were more accurately calculated. The hardening caused by the dislocation loops was revealed to be comparable with that by solute clusters, which provides important insight into understanding the embrittlement mechanism in RPV steels.

The International Research Center for Nuclear Materials Science (IRCNMS) is the leading and globally opened center in Japan for research of nuclear materials and actinides. A collaboration between IRCNMS and the Belgian Nuclear Research Center as a new breakthrough on the life prediction of light-water reactor materials.

The irradiation embrittlement of reactor pressure vessel (RPV) steels is a vital issue for ensuring the safe operation of plants. Numerous studies have revealed that the origins of embrittlement are dislocation loops and solute clusters. Both are induced by long-term neutron irradiation. Contributions of solute clusters have been identified as a main cause of the hardening using atom probe tomography in the 2010's. However, the irradiation-induced small dislocation loops does not show any sufficient determination for their roles in the embrittlement.

Recently, IRCNMS developed the weak-beam scanning transmission electron microscopy (WB-STEM) [1], which makes it possible to quantify such dislocation loops with higher resolution and without interference artifacts in a large field of view. It provides considerable accuracy about the number density measurement of dislocation loops. We firstly applied the WB-STEM to various RPV surveillance test specimens to quantify the number densities of irradiation-induced dislocation loops, together with atom probe tomography and positron annihilation spectroscopy [2].

Low-Cu surveillance test specimens of a European pressurized water reactor were irradiated to the fluences of 1.3×10^{23} , 3.4×10^{23} , 8.2×10^{23} , and 1.2×10^{24} n m^{-2} , called T1–T4, respectively. Solute clusters were densely formed in the high fluences (T3 and T4) at a number density of $\sim 3 \times 10^{23} \text{ m}^{-3}$. The estimated hardening caused by solute clusters was more than half of the actual hardening, indicating that solute clusters should be a main source of hardening in the high fluences. However, dislocation loops also formed in the high fluences (T3 and T4), as shown in Fig. 1. The average size was ~ 4 nm

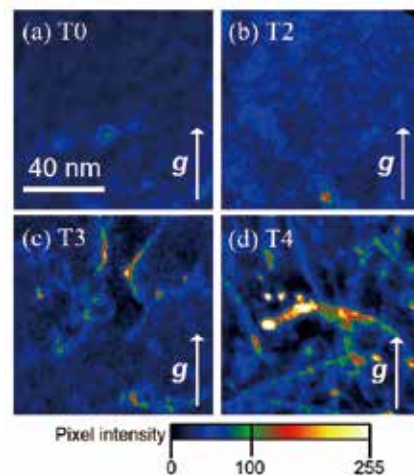


Fig. 1(a)–(d) Color intensity maps of WB-STEM images for surveillance test specimens — (a) unirradiated, and (b)–(d) irradiated to the fluences of 3.4×10^{23} n m^{-2} (T2), 8.2×10^{23} n m^{-2} (T3), and 1.2×10^{24} n m^{-2} (T4)

in diameter both for T3 and T4, and the number densities were $1.3 \times 10^{22} \text{ m}^{-3}$ in T3 and $3.4 \times 10^{22} \text{ m}^{-3}$ in T4. These number densities are approximately three times higher than those in previous reports, implying the advantage of WB-STEM. The hardening resulting from the dislocation loops was also estimated, and it was revealed that the contribution of the dislocation loops is comparable to that caused by solute clusters. This is an important insight for a more-precise understanding of the embrittlement mechanism in RPV steels, especially in high fluences.

References

- [1] K. Yoshida, M. Shimodaira, T. Toyama, Y. Shimizu, K. Inoue, T. Yoshiie, K. J. Milan, R. Gerard, and Y. Nagai, *Microsc.* **66**, 120 (2017).
- [2] M. Shimodaira, T. Toyama, K. Yoshida, K. Inoue, N. Ebisawa, K. Tomura, T. Yoshiie, M. J. Konstantinovic, R. Gerard, and Y. Nagai, *Acta Mater.* **155**, 402 (2018).

Keywords: nuclear materials, radiation effects, STEM

Yasuyoshi Nagai (Head of International Research Center for Nuclear Materials Science)

E-mail: nagai@imr.tohoku.ac.jp

URL: <http://www.imr-oarai.jp/>

Fabrication of Non-Equilibrium Mono-Dispersed Particles by Container-Free Solidification Process and Their Applications

Cooperative Research and Development Center for Advanced Materials

The Cooperative Research and Development Center for Advanced Materials has contributed to the research and development of new materials and their fabrication processes to explore the possibility of their application as multi-functional materials for future technologies under collaboration with universities and National research institutes. Herein, we highlight our recent research and development activities on non-equilibrium alloys for industrial application.

We study non-equilibrium alloys such as amorphous alloys, metallic glasses, and nanocrystal alloys along with other institutes and private companies [1-4].

A container-free solidification process enables molten alloys to quench a non-equilibrium structure under an environment where nucleation is suppressed. In our research, mono-dispersed particles were fabricated using a container-free solidification process called a pulsated orifice ejection method (POEM).

Figure 1 shows the outer appearance of Fe-based metallic glassy mono-dispersed particles with a 370 μm diameter. It can be confirmed that the particles obtained have a spherical shape and are uniform in size. We also developed a high-precision micro-viscous flow processing technique using a single particle, and an evaluation method for the soft magnetic properties of nanostructured materials by applying a single spherical particle. Figure 2(a) shows an SEM image of the micro-gear prepared through our micro-viscous flow process as a representative micro-component. It was confirmed that the micro-component produced consists of a single amorphous phase and shows excellent mechanical properties. Figure 2(b) illustrates the heat treatment temperature dependency of the saturation magnetic flux density of a single Fe-based particle. Using our method, the number of inner nucleation sites is reduced in an as-quenched state, resulting in homogenous nanocrystalline grains after optimum annealing.

Our process has superiority regarding the preparation of Fe-based metallic glasses with a low glass forming ability. We are currently attempting to find a new application with other alloy systems using this technology.

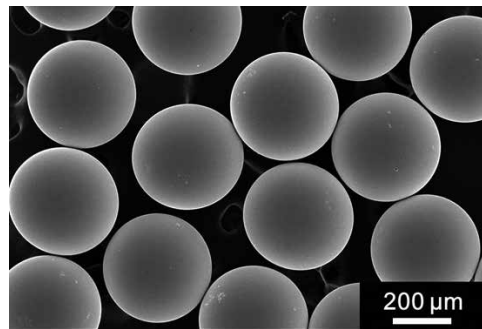


Fig. 1 Outer appearance of Fe-based metallic glassy mono-dispersed particles of 370 μm in diameter prepared using a pulsated orifice ejection method.

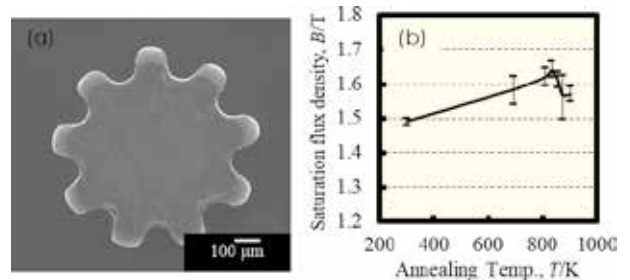


Fig. 2 (a) SEM image of a micro-gear prepared using our micro-viscous flow process as a representative micro-component, and (b) heat treatment temperature dependency of saturation magnetic flux density of single Fe-based particle.

References

- [1] N. Yodoshi, S. Ookawa, R. Yamada, N. Nomura, K. Kikuchi, and A. Kawasaki, *Mater. Res. Lett.* **6**(1), 100 (2018).
- [2] N. Yodoshi, S. Ookawa, R. Yamada, A. Kawasaki, and A. Makino, *J. Alloy. Comp.* **679**, 164 (2016).
- [3] J. Luan, P. Sharma, N. Yodoshi, Y. Zhang, and A. Makino, *AIP Adv.* **6**, 55934 (2016).
- [4] N. Yodoshi, R. Yamada, A. Kawasaki, *Materia* **55**(4), 152 (2016).

Keywords: metallic glass, nanostructure, magnetic properties

Noriharu Yodoshi (Cooperative Research and Development Center for Advanced Materials)

E-mail: ynoriharu@imr.tohoku.ac.jp

Naoya Masahasi (Head of Cooperative Research and Development Center for Advanced Materials)

E-mail: crdam@imr.tohoku.ac.jp

URL: <http://www.crdam.imr.tohoku.ac.jp>

2.5-GPa 25-T High-Pressure High-Field Electron Spin Resonance System Using a Cryogen-Free Superconducting Magnet

High Field Laboratory for Superconducting Materials

Combining multiple extreme conditions is the one of the most effective ways to investigate quantum phase transitions of matter. Here, the development of a 2.5-GPa high-pressure electron spin resonance probe with the world's highest-field cryogen-free superconducting magnet, whose maximum field reaches 24.6 T, is reported. It was used to investigate a quantum phase transition of the orthogonal dimer spin system $\text{SrCu}_2(\text{BO}_3)_2$.

The orthogonal dimer spin system $\text{SrCu}_2(\text{BO}_3)_2$ shows a unique dimer ground state that is given by the product of isolated dimer wave functions despite the strong exchange couplings acting among two-dimensional arrays of $S = 1/2$ spins. The decoupling is caused by strong frustration between two exchange couplings in a triangular unit composed of two dimers connected by large intradimer interaction. The magnitude of the frustration depends on the ratio of two exchange interactions, and the exact dimer singlet ground state dominates the large range of the parameter space. Theoretically, another type of singlet state called the “plaquette state” is expected above the critical value between the interdimer and intradimer interactions. However, an experimental verification has not been established yet.

To attack this long-standing problem, a few points must be qualified experimentally. The first one is the modulation of the exchange couplings by the application of high pressure. This gives the most clean and straight way to modify the ratio of exchange parameters. According to the structural investigation under high pressure, the application of more than 2 GPa required. The second point is high magnetic fields of 25 T. This field is needed to close the singlet–triplet gap by the Zeeman effect. The third point is the observation of energy levels by using an electron spin resonance. The last point is very important, because this phase transition is the change between two types of singlet state. Such a transition cannot be examined by conventional magnetic measurements, such as magnetization or susceptibility. It should be stressed that the present target can be achieved only by combining these advanced extremes and techniques.

A Kobe University group has developed electron spin resonance under high pressure by using pulsed magnetic fields and found the trace of the expected phase transition. However, the heating



Fig. 1 High-pressure cell used for the electron spin resonance experiment

by an eddy current, which cannot be avoided in the combination of a high-pressure cell and a pulsed magnetic field, has made a clear and complete conclusion difficult. However, a magnetic field provided by superconducting magnets was not enough until the installation of a 25-T superconducting magnet at the High Field Laboratory for Superconducting Materials [1].

Figure 1 shows a picture of the high-pressure electron spin resonance cell used in the experiments. By installing the cell into a 25-T magnet, the loss of the pressure dependence of the singlet–triplet gap at approximately 1.85 GPa was observed. Additional evidence was given by the enhancement of the singlet–triplet mixing by high-pressure application. These two clear changes of spin excitations indicate the existence of the expected quantum phase transition by the high pressure. The present study shows the power of the 25-T superconducting magnet for studies of matter in multiple extreme conditions.

References

- [1] T. Sakurai, S. Kimura, M. Kimata, H. Nojiri, S. Awaji, S. Okubo, H. Ohta, Y. Uwatoko, K. Kudo, and Y. Koike, *J Magn. Reson.* **296**, 1 (2018).

Keywords: high magnetic field, high pressure, quantum phase transition

Takahiro Sakurai and Hitoshi Ohta (Corresponding Authors, Kobe University)

E-mail: tsakurai@kobe-u.ac.jp

Hiroyuki Nojiri and Shojiro Kimura (High Field Laboratory for Superconducting Materials)

E-mail: nojiri@imr.tohoku.ac.jp

URL: <http://www.hflsm.imr.tohoku.ac.jp/cgi-bin/index.cgi>

Self-Sufficient Material Circulation System Driven by Plasma Generated in Aqueous Phase

Trans-Regional Corporation Center for Industrial Materials Research

When applying a short-pulsed high voltage with a high repetition frequency to metal electrodes placed in water, plasma (glow discharge) can be generated. Herein, we show the projection of a material circulation system driven by plasma, aiming to establish a self-sufficient community.

We have been investigating applications of discharge plasma generated in water. We developed a plasma system available for continuous flow water treatment, which is difficult with a conventional plasma generation method. [1]. Owing to the Venturi effect, air was introduced to a water flow (at typically several liters per minute) between a couple of metal electrodes to generate stable plasma with a relatively low breakdown voltage. N₂ in air was decomposed, oxidized, and finally dissolved as nitrate ions in the plasma-treated water. Therefore, as shown in Fig. 1, the plasma-treated water can be utilized as a nutrient solution in a hydroponic culture. It is important to prevent plants from up-taking heavy metals released from electrodes or piping materials because they cause a significant inhibition in growth.

Plasma can be utilized for the sterilization of water. When Ag wires were used as electrodes for plasma generation, the treated water contained AgNO₃ with a very low concentration, which maintained a sterilization effect against *Trichophyton* and *Escherichia coli* for several months. Sterilization is important in a hydroponic culture to prevent plant disease. In addition, the restriction of an algal exuberance is an important issue in a hydroponic culture mainly owing to the sensuousness. Stable plasma can be generated even in high conductive water such as seawater using a flow plasma generation system. Diatoms in seawater, namely, *Chaetoceros gracilis* and *Chaetoceros calcitrans*, were successfully deactivated [2]. The sterilization or deactivation is considered to originate from direct contact of algae or bacteria with the plasma core, and the contribution of *in-situ* formed reactive species such as OH radicals, peroxyxynitrite, and AgNO₃.

Using a batch plasma system, the generation of plasma in an aqueous NH₃ solution effectively



Fig.1 Barley (*Hordeum vulgare* L. cv. Wasedori) cultivated for 8 days in (a) tap water and (b) plasma-treated water. Approximately 30% growth promotion was observed in (b).

decomposes NH₃ molecules to provide N₂ and H₂ gases with an almost stoichiometric molar ratio [3]. This means that plasma treatment is an effective NH₃ removal method in waste water, and an effective H₂ production method from an aqueous NH₃ solution. Because the urea contained in urine is converted into NH₃ through hydrolysis or enzymatic decomposition, the plasma treatment is expected to be utilized in the conversion of human waste into H₂.

By integrating the above processes, we can simultaneously reduce human waste, cultivate crops, and store H₂ energy. The promotion of this material circulation through plasma is expected to contribute to maintaining the “quality of life” in enclosed environments such as disaster shelters, space ships, and space colonies, among others.

References

- [1] Y. Mizukoshi, R. Katagiri, H. Horibe, S. Hatanaka, M. Asano, and Y. Nishimura, *Chem. Lett.* **44**, 495 (2015).
- [2] Y. Mizukoshi, Y. Matsuda, S. Yamanaka, T. Ikeno, K. Haraguchi, N. Goda, Y. Nishimura, and K. Yamamoto, *Chem. Lett.*, **47** 116 (2018).
- [3] Y. Mizukoshi, S. Hatanaka, K. Okitsu, Y. Iseki, R. Iwasaki, T. Sakamoto, S. Yamaguchi, H. Tanaka, and S. Tanabe, *Jpn. J. Appl. Phys.* **57**, 0102B7 (2018).

Keywords: glow discharge plasma, hydrogen evolution

Yoshiteru Mizukoshi (Corresponding Author, Trans-Regional Corporation Center for Industrial Materials Research)

E-mail: mizukosi@imr.tohoku.ac.jp

Naoya Masahashi (Head of Trans-Regional Corporation Center for Industrial Materials Research)

E-mail: masahasi@imr.tohoku.ac.jp

URL: <http://www.trc-center.imr.tohoku.ac.jp/>

Energy Simulation Model for Disaster Prevention System by Using Renewable Energy and Hydrogen Energy

Collaborative Research Center on Energy Materials

A new energy management for disaster prevention system to use surplus energy from a solar power and battery life extension method is being developed in Sendai City to apply to facilities such as designated evacuation centers during a disaster. The energy simulation model for this disaster prevention program by using hydrogen energy technology to store a large amount of electricity is also examined.

Based on the experience of the 2011 Tohoku earthquake and tsunami, Sendai City is proceeding to establish a “Disaster-Resilient and Environmentally-Friendly City” and actively create a base for disaster-resistant, energy-efficient decentralized energy sources. It is also introducing renewable energy sources. Sendai City introduced a disaster prevention solar system equipped with a solar power generation system and a storage battery for 194 facilities as designated evacuation centers during a disaster. This disaster prevention solar system does not utilize CO₂-free electricity generated from solar power at weekends and holidays, and the battery of this system is always fully charged, which causes a battery life problem. A collaboration with Sendai City is under way for developing new energy management for next-generation disaster prevention by using surplus energy from solar power and applying a battery life extension method, as shown in in Fig. 1 [1]. In this project, a model will be built for deployment to a virtual power plant. In September 2018, a joint research agreement was reached with Sendai City and the Japan Weather Association for enhancing this energy management technology based on detailed weather forecast data [2]. Today's weather conditions are used for power demand forecasting for the facility as research for environmental improvement, and surplus power is assumed based on tomorrow's solar radiation forecast data, and it is put in control. Also, in research aimed at improving disaster prevention, the solar radiation forecast data for tomorrow will be reflected in the storage capacity of the battery, and charging of the battery will be secured immediately in response to the weather warning.

A hydrogen system is one of the most effective ways to improve a conventional battery system from the viewpoint of volumetric energy density (Wh/L). An energy simulation model is being developed for this disaster prevention system by using a hydrogen energy system to store a large amount of electricity, as in in Fig. 2. For storing a large amount of hydrogen safely and easily in

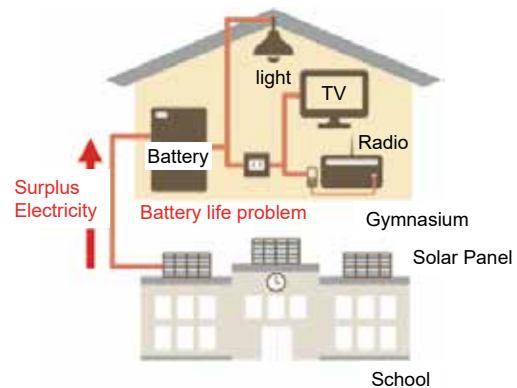


Fig. 1 Disaster prevention solar system

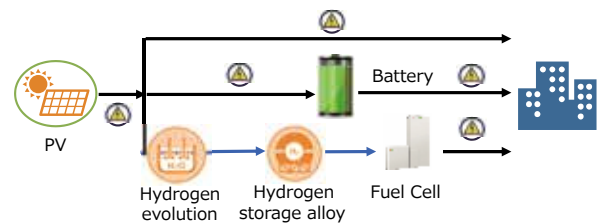


Fig. 2 Disaster prevention solar system by adapting hydrogen energy

this system, hydrogen storage alloy technology is the key issue compared with a conventional high pressure hydrogen gas tank. A new hydrogen storage alloy having a high hydrogen storage capacity is also being studied to apply to this energy system. In the future, it is planned to improve this simulation model, establish scenarios using real equipment, and proceed with an attempt to construct a system concept.

References

- [1] https://www.tohoku.ac.jp/japanese/newimg/pressimg/tohokuuniv-press20180508_01_zisedaibosai.pdf (2018).
- [2] https://www.tohoku.ac.jp/japanese/newimg/pressimg/tohokuuniv-press20180927_01web_kishoujouhou.pdf (2018).
- [3] T. Kono, J. Hydrogen Energy Syst. Soc. Jpn. **42(4)**, 218 (2017).

Keywords: energy storage, hydride, hydrogen evolution
 Tatsuoki Kono (Collaborative Research Center on Energy Materials)
 E-mail: tatsuoki@imr.tohoku.ac.jp
 Shin-ichi Orimo (Head of Collaborative Research Center on Energy Materials)
 E-mail: orimo@imr.tohoku.ac.jp
 URL: <http://www.e-imr.imr.tohoku.ac.jp/process.html>

Understand Materials Properties and Find New Materials by Supercomputer

Center for Computational Materials Science

The Center for Computational Materials Science supports various advanced studies on computational materials science by providing users with an efficiently tuned high-performance computer. We introduced two major activities selected from approximately 150 users. Dr. Chen investigates the optical properties of dense lithium in electride phases, and Dr. Kawazoe finds new carbon allotropes.

First-principles Study of Optical Properties of Dense Lithium in Electride Phases^{a)}

Pressure alters the state of matter by squeezing electrons into a smaller space and modifying the interactions between particles. It is not surprising that metals are usually anticipated to become more “metallic” at high pressure owing to expected broadening of the bandwidth and an overlapping of the electronic orbitals. Lithium, as the simplest metallic element, demonstrates how pressure turns a metal into an insulator and induces some intricate and fascinating properties. We calculated the dynamic dielectric response, reflectivity, and electron energy-loss spectroscopy of high-pressure electride phases of cI16, oC40, and oC20 of Li (Fig. 1), spanning a wide pressure range using first-principles calculations, which resulted in the following new findings [1]: 1) One intraband and two interband excitations in cI16 are induced through a structural distortion, which leads to an abnormally low reflectivity of this weak metallic phase, 2) oC24 as a reentrant metallic phase with a high light conductivity in the infrared and visible light ranges point to its unique electronic structure around a Fermi surface, and 3) an intriguing reflectivity anisotropy in both oC40 and oC24. The origin of such diversity and rich physics in Li electrides can be attributed to the interplay between interstitial electron localization and delocalization induced through compression, which leads to exotic electride phases.

How to Find New Carbon Allotropes^{b)}

It has been a dream to find new single element carbon system theoretically prior to experiments. We theoretically found Mackay-like structures, which are extremely stable, and some of which are topological insulators [2]. In the first case, only single element material realizes topological insulator. In the same year, we found another material, penta-graphene (Fig. 2) [3], which is composed of pentagones with a mixture of sp^2 and sp^3 bondings. This completely new structure of thin film carbon allotrope is stable and has many interesting properties, the most important one is negative Poisson's ratio

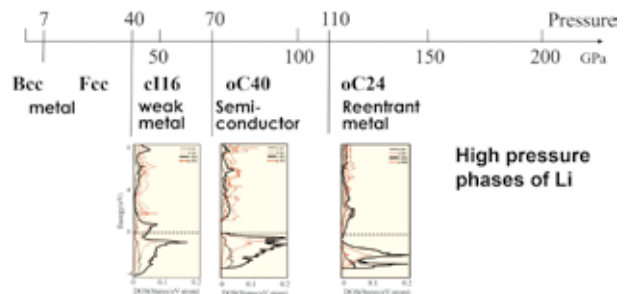


Fig. 1 High-pressure phases and calculated density of states (DOS) in lithium.

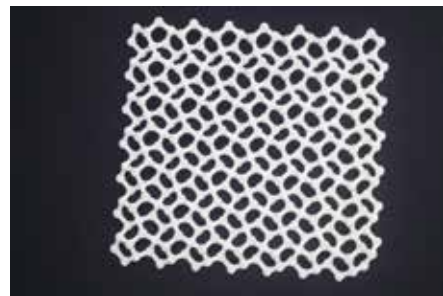


Fig. 2 Penta-graphene

(penta-graphene is the first stable material having a negative Poisson's ratio, which can help realize new materials that do not deform under pressure (the geometry of which is the most important) and therefore applicable for macroscopic cases). These have been continuously highly cited papers in these 3 years, and experimentally realized in some extent. We have recently started to apply the materials informatics (MI) method to find more interesting materials theoretically.

References

- [1] Z. Yu, H. Y. Geng, Y. Sun, and Y. Chen, *Scientific Reports* **8**, 3868 (2018).
- [2] H. Weng, Y. Liang, Q. Xu, R. Yu, Z. Fang, X. Dai, and Y. Kawazoe, *Phys. Rev. B* **92**, 45108 (2015)
- [3] S. H. Zhang, J. Zhou, Q. Wang, X. S. Chen, Y. Kawazoe, and P. Jena, *PNAS* **112**, 2372 (2015)

Keywords: optical properties, first-principles calculations, simulation

a) Ying Chen (Corresponding Author, School of Engineering, Tohoku University)

E-mail: ying@rift.mech.tohoku.ac.jp

b) Yoshiyuki Kawazoe (Corresponding Author, New Industry Creation Hatchery Center, Tohoku University)

E-mail: kawazoe@niche.tohoku.ac.jp

Momiji Kubo (Head of Center for Computational Materials Science)

Email: momoji@imr.tohoku.ac.jp

URL: <https://www.sc.imr.tohoku.ac.jp/eng/>

Scintillation Properties of Mg²⁺-Codoped (Lu_xGd_{3-x})Al_{2.4}Ga_{2.6}O₁₂:Ce Multicomponent Garnet Crystals

International Collaboration Center (ICC-IMR)

The scintillation properties of Mg²⁺-codoped (Lu_xGd_{3-x})Al_{2.4}Ga_{2.6}O₁₂:Ce ($x = 0.2 - 0.8$) crystals grown by micro-pulling down method are reported. Acceleration of scintillation decays with an expense of light yield (LY) is obtained with increasing Lu content. LGAGG:Ce,Mg ($x = 0.8$) exhibits high LY of 32,000 photons/MeV, dominant decay time of 52 ns, and coincidence time resolution of 400 ps.

The positive role of Ce⁴⁺ centers stabilized by Mg²⁺ - codoping has been proposed to explain the shortening of scintillation decay time in Gd₃Al₂Ga₃O₁₂:Ce [1,2] and Lu₁Gd₂(Ga,Al)₅O₁₂ [3] garnet crystals. In this work the Mg 500 ppm codoped (Lu_xGd_{3-x})Al_{2.4}Ga_{2.6}O₁₂:Ce0.5% ($x = 0.2-0.8$) crystals were grown by the micro-pulling down method using Ir crucible under Ar + 2% O₂ atmosphere at the IMR, Tohoku University, Japan.

The blue-shifted of RL band (Fig.1) was observed with increasing Lu content in the same trend with the 4f→5d₁ absorption band (not shown). This result can be explained by a decrease of crystal field strength around Ce³⁺ at the dodecahedral site of (Lu_xGd_{3-x})AGG:Ce crystal upon partial substitution of Gd³⁺ with a smaller Lu³⁺ ion. Scintillation decays and energy spectra of ¹³⁷Cs γ rays for LGAGG:Ce,Mg are displayed in Figs. 2 and 3, respectively. With increasing Lu content, decay time shortening and decrease of light yield can be attributed to a blue-shifted emission spectrum ($\tau \sim \lambda^3$) and a larger bandgap caused by a high-energy shift of the bottom of the conduction band [4,5], respectively. It is worthy to note that a decay time of 52 ns obtained for Lu_{0.8}Gd_{2.2}AGG:Ce,Mg sample is faster than that of 68 ns for Lu_{0.8}Gd_{2.2}AGG:Ce one.

LGAGG:Ce,Mg ($x = 0.2$) crystal exhibits high LY of 36,500 ph/MeV and dominant decay time of 62 ns whereas those values of 32,000 ph/MeV and 52 ns are obtained for the LGAGG:Ce,Mg ($x = 0.8$) one. Coincidence time resolution of 400 ps was also measured for the LGAGG:Ce,Mg ($x = 0.8$). Further improvement of the scintillation timing characteristics could be achieved by optimization of Ga/Al ratio and concentration of Mg codopant.

References

- [1] M. Nikl et al., *Cryst. Growth Des.* **14**, 4827 (2014).
 [2] K. Kamada et al., *Opt. Mater.* **41**, 63(2015).

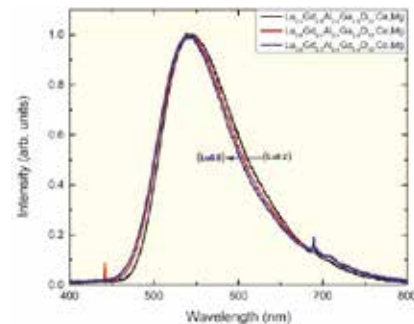


Fig. 1 RL spectra of selected LGAGG:Ce,Mg crystals.

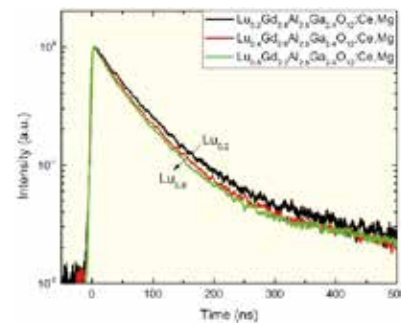


Fig. 2 Scintillation decays of selected LGAGG:Ce,Mg crystals.

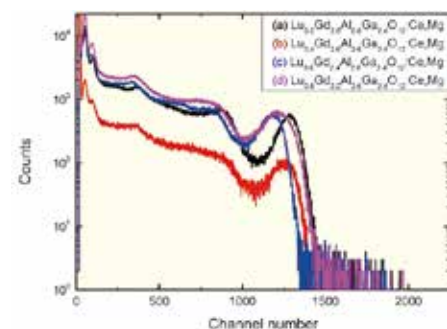


Fig. 3 Pulse height spectra of ¹³⁷Cs γ rays measured with LGAGG:Ce,Mg crystals.

- [3] H. Yamaguchi et al., *Opt. Mater.* **61**, 129 (2016).
 [4] L. Chen et al., *Sci. Rep.* **5**, 11514 (2015).
 [5] W. R. Chewpraditkul et al., *Opt. Mater.* **76**, 162 (2018).

Keywords: (Lu,Gd)₃AGG:Ce, Mg, light yield, scintillation decays
 Weerapong Chewpraditkul (King Mongkut's University of Technology Thonburi)
 Email: weerapong.che@kmutt.ac.th
 Gerrit Ernst-Wilhelm Bauer (Head of International Collaboration Center)
 E-mail: icc-imr@imr.tohoku.ac.jp
 URL: <http://www.icc-imr.imr.tohoku.ac.jp/>

Starting Collaborative Research Programs of CNSAM

Center of Neutron Science for Advanced Materials

The Center of Neutron Science for Advanced Materials is a neutron facility, which has a background of novel materials science in IMR. This center operates three neutron instruments in a research reactor facility, JRR-3, under a general user program, and will start a new user program for a brand-new spectrometer, POLANO, at J-PARC/MLF in April 2019. Herein, we report the current status of POLANO.

The Center of Neutron Science for Advanced Materials (CNSAM) was established in 2010 to promote novel materials science research using neutrons. CNSAM operates two neutron spectrometers and one diffractometer at the JRR-3 research reactor of the Japan Atomic Energy Agency and has been constructing a polarized neutron spectrometer, POLANO, with an intense neutron source at the Materials and Life Science Experimental Facility (MLF) in the Japan Proton Accelerator Research Complex (J-PARC) [1]. POLANO is a brand-new spectrometer designed to realize a polarization analysis in higher energy regions beyond the measurements achieved through a conventional triple-axis spectrometer. The construction of POLANO was initiated in 2012 under collaboration with the High Energy Accelerator Research Organization (KEK). After the construction of the main part of the instruments [2], we finally succeeded in receiving the first neutron beam at POLANO in June 2017 and started on-beam commissioning.

Figure 1 shows the results of the test measurements of position-sensitive detectors. The colors represent the neutron intensity. The scattered neutrons from a standard sample can be successfully detected. Using the data obtained, the efficiency of the detectors was calibrated. Furthermore, we installed equipment including a Fermi chopper at POLANO to carry out inelastic scattering measurements. Figure 2 (c) shows the representative results of the measured magnetic excitation spectrum from a one-dimensional spin system, CsVCl₃. As the figure indicates, a spin-wave excitation of up to ~80 meV was clearly observed. Thus, POLANO can provide an opportunity to study the spin and lattice dynamics in novel materials. We have prepared collaborative research programs of IMR to support the experiments conducted at POLANO, in accordance with the beginning of a general user program of POLANO at J-PARC MLF.

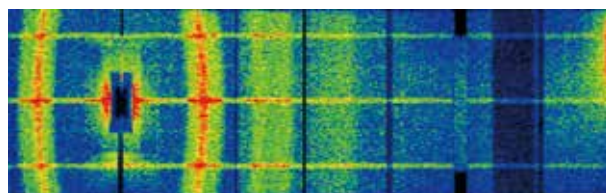


Fig. 1 Neutron intensity map measured using position sensitive detectors of POLANO.

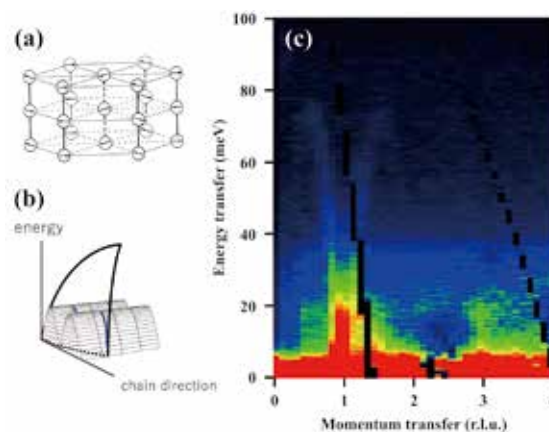


Fig. 2 (a) Crystal and magnetic structures of CsVCl₃. (b) Scan trajectory of neutron inelastic measurements for one-dimensional magnetic system. (c) Magnetic excitations for CsVCl₃ at POLANO.

References

- [1] T. Yokoo, S. Itoh, N. Kaneko, M. Fujita, T. Ino, M. Ohkawara, K. Ohyama, and M. Sakaguchi, AIP Conf. Proc. **1969**, 050001 (2018).
- [2] M. Ohkawara, T. Ino, Y. Ikeda, T. Yokoo, S. Itoh, K. Ohoyama, and M. Fujita, JPS Conf. Proc. **22**, 011017 (2018).

Keywords: neutron scattering, instrumentation, spin excitation

Masaki Fujita (Head of Center of Neutron Science for Advanced Materials)

E-mail: nc-imr@imr.tohoku.ac.jp

URL: <http://nc-imr.imr.tohoku.ac.jp/>

Spin Trimer Formation in the Metallic Compound $Gd_3Ru_4Al_{12}$ with a Distorted Kagome Lattice Structure

Laboratory of Low Temperature Materials Science

We demonstrate the gradual formation of ferromagnetic trimers on a distorted (breathing) kagome lattice with decreasing temperature in $Gd_3Ru_4Al_{12}$ single crystals. This trimerization can induce an antiferromagnetic intertrimer interaction and lead to an effective transformation into an antiferromagnetic triangular lattice with frustration at low temperature.

$RE_3Ru_4Al_{12}$ (RE = rare earth element) compounds have been investigated intensively in recent years because they display a variety of phenomena at low temperatures as metallic frustrated $4f$ spin systems with spin multimers. Among them, the puzzling magnetism features of $Gd_3Ru_4Al_{12}$, showing a Curie-Weiss temperature of +80 K at high temperatures despite the antiferromagnetic (AFM) order at low temperatures, are an open problem [1].

We have succeeded in synthesizing single crystals of $Gd_3Ru_4Al_{12}$, which exhibits a distorted kagome lattice [2]. This lattice includes small and large regular triangles of Gd ions, which are responsible for the magnetic properties, as shown in Fig. 1(a). Measurements of the magnetic susceptibility and magnetic specific heat indicate that ferromagnetic spin trimers are gradually formed on the small triangles with a decrease in temperature through an RKKY interaction at below 130 K. This formation of ferromagnetic trimers induces an AFM inter-trimer interaction between the nearest-neighbor trimers based on the oscillatory features of an RKKY interaction. As a result, $Gd_3Ru_4Al_{12}$ translates into an AFM triangular lattice at low temperatures, as shown in Fig. 1(b). The magnetic entropy at the Neel temperature of $Gd_3Ru_4Al_{12}$ is only 40% of the full magnetic entropy. In this compound, the generation of ferromagnetic clusters (trimers) induces frustration and significantly reduces the Neel temperature.

References

- [1] V. Chandragiri, K. K. Iyer, and E. V. Sampathkumaran, *J. Phys. (Cond. Mat.)* **28**, 286002 (2016).
 [2] S. Nakamura, N. Kabeya, M. Kobayashi, K. Araki, K. Katoh, and A. Ochiai, *Phys. Rev. B* **98**, 054410 (2018).

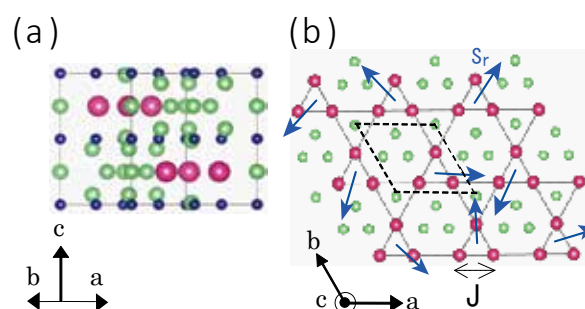


Fig. 1 (a) Structure of $Gd_3Ru_4Al_{12}$ projected parallel to the ab plane. The red, blue, and light green spheres denote Gd, Ru, and Al ions, respectively. (b) A Gd-Al layer projected parallel to the c -axis. The blue arrows indicate the resultant spin, S_r ($S_r = 21/2$).

Keywords: magnetism, frustrated spin system

Shintaro Nakamura (Laboratory of Low Temperature Materials Science)

E-mail: nakamura@imr.tohoku.ac.jp

Takahiko Sasaki (Head of Laboratory of Low Temperature Materials Science)

E-mail: takahiko@imr.tohoku.ac.jp

URL: <http://itsd.imr.tohoku.ac.jp/>

Research Facility for Physics and Chemistry of Radioactive and Nuclear Materials:

Laboratory of Alpha-Ray Emitters

More than 170 species of radioisotopes and nuclear materials are available for study at the Laboratory of Alpha-Ray Emitters. This laboratory is one of the most important centers around the world for studying the physical and chemical properties of radioactive materials, such as actinide compounds. Researchers from many of the leading universities and institutes all over Japan visit this facility every year to prepare a variety of materials and carry out chemical and physical measurements.

The Laboratory of Alpha-Ray Emitters provides a research environment for the study of 170 radionuclides and nuclear materials, especially alpha-ray emitters, such as actinide. This lab functions as a source for the preparation of pure crystals of actinide compounds, providing them to other universities and to synchrotron orbital radiations. The radiation controlled area of this laboratory includes three chemistry rooms, three physical rooms, and so on, which are equipped with local exhaust ventilation systems making the handling of various kinds of material possible. Many spectrometers, including those for gamma rays and alpha rays, are available.

In the past decade, actinium-225 (Ac-225), one of the actinide elements, has been reported because of its effectiveness for medical use [1, 2]. Ac-225 (half-life: 10 d) decays through a chain of four alpha emissions and two beta-minus emissions to the stable isotope Bi-209. The decay process releases ~28 MeV of energy to the surrounding media with changing of the element, and the chain does not involve noble gas, which is a chemically uncontrollable element. All of these nuclide properties seem to be suitable for the treatment of tumors, and Ac-225 is actually used in clinical practice outside the country. Although it is a testament to the effectiveness of radiopharmaceuticals, very limited investigation has been done in Japan. One of the main reasons is that Ac-225 is subject to rigid regulation as an alpha-ray emitter. In this study, the aim was to evaluate the dispersion of Ac-225 and its progeny nuclides. This evaluation is especially important for establishing a guideline for the control standard, especially for Ac-225 practical use.

For obtaining a starting material of Ac-225, a Th-229 milking method was used. This material, composed of 10 mL of 0.05-M HNO₃ aq. containing Ac-225, adjusted to the conditions of the dispersion

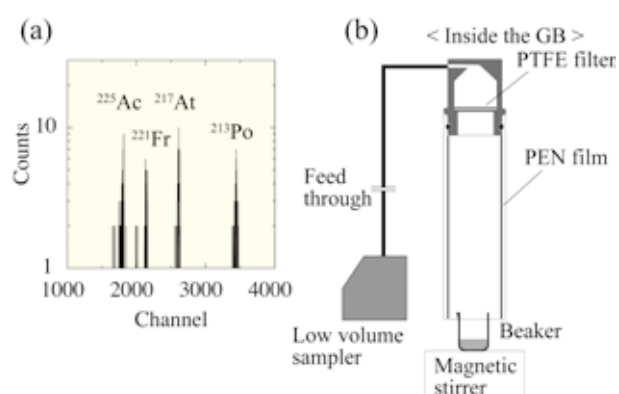


Fig. 1 Alpha-ray spectra of Ac-225 and its progeny nuclides obtained from standard sample (a) and dispersion evaluation system (b). In the container, two PTFE filters were placed downstream from the air inlet. The container was set at the top of an acrylic cylinder (70-mm i.d., 80-mm o.d., and 480-mm length), and inner aspect of the acrylic cylinder was filled using a PEN film.

experiments (liquid: acidic, neutral, and neutral complex solutions, solid: nitric acid salt). The dispersion experiments were carried out using a special composition of sampling for alpha-ray spectroscopic identification (Fig. 1). Just after the aspiration, typically 1 h, PTFE filters and some part of PEN film were ejected from the apparatus and measured by an alpha-ray spectrometer.

The dispersion rate of Ac-225 and its progeny nuclides was well identified. The dispersion rate was obtained in descending order, neutral complex > neutral > acidic, in the liquid condition. Even in the highest, the dispersion rate was less than 10⁻⁴/h, which is 1/100 of the typically used value.

References

- [1] C. Kratochwil *et al.*, J. Nucl. Med. **57**, 1941 (2016).
- [2] C. Kratochwil *et al.*, J. Nucl. Med. **59**, 795 (2018).

Keywords: actinide, alpha-ray spectroscopy, short-life alpha-ray emitter

Kenji Shirasaki (Head of Laboratory of Alpha-Ray Emitters)

E-mail: kshira@imr.tohoku.ac.jp

URL: <http://alpha.imr.tohoku.ac.jp>

Synthesis, Crystal Structure, and Luminescence Properties of a New Nitride Polymorph, β -Sr_{0.98}Eu_{0.02}AlSi₄N₇

Analytical Research Core for Advanced Materials

A novel strontium aluminum silicon nitride phosphor, namely, a β -Sr_{0.98}Eu_{0.02}AlSi₄N₇ single crystal, which emits green light under excitation at 400 nm, was fabricated. Because identifying its crystal structure using only XRD is quite difficult owing to the twin-defects contained in the specimen, TEM and STEM-HAADF techniques using the latest Cs-corrected electron microscope were employed herein to characterize the detailed crystal structure.

SrAlSiN₇ doped with Eu²⁺ has been reported as a phosphor material for use in combination with near ultraviolet light and a blue light LED to realize a backlight of a liquid crystal display or a white LED. This nitride belongs to an orthorhombic structure and exhibits a red emission with a broad peak at a wavelength of 635 nm under an excitation light of 450 nm [1]. In the present study, we synthesized vermilion prismatic and yellow platelet single crystals having similar chemical compositions from a mixture of Sr₃N₂, Mg₃N₂, EuN, AlN, and α -Si₃N₄ powders by heating at up to 800–2030 °C under a N₂ atmosphere. The vermilion crystals emitted red light, whereas the yellow crystals emitted green light under excitation at 400 nm. A single-crystal XRD confirmed that the vermilion crystals are α -SrEuAlSiN₇ and suggested that the yellow crystals are new polymorph containing twin defects [2].

Therefore, analyses on the twin-boundary structure and an identification of the unit cell of the new polymorph have been conducted using S/TEM. High-resolution TEM observations indicated the existence in a single crystal specimen with twin bands at a thickness of tens of nanometers, as shown in Fig. 1(c). The SAD pattern taken from the twin-contained region exhibited a mirror symmetry, as shown in Fig. 1(a), which is consistent with the XRD results; in addition, using a small selected-area aperture, the pattern from a single crystal region could also be obtained, as shown in Fig. 1(b). Furthermore, direct observations of the atom arrangement using HAADF-STEM revealed that the unit cell of the new polymorph consists of the stacking of two types of layers, including and not including heavy Sr/Eu atoms, labeled A and B, respectively, in Fig. 1(d). Thus, we concluded that the new polymorph, β -Sr_{0.98}Eu_{0.02}AlSi₄N₇,

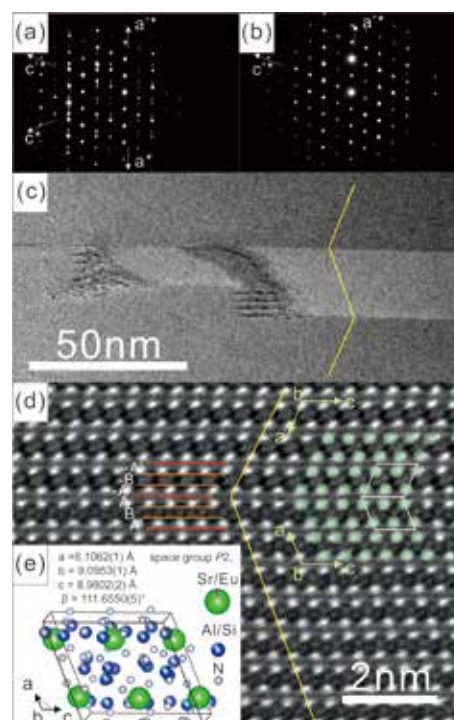


Fig. 1 SAD patterns from (a) twin and (b) single regions, and (c) HREM and (d) HAADF-STEM images taken from the [010] direction in β -Sr_{0.98}Eu_{0.02}AlSi₄N₇ crystal (inset (e) schematic drawing of corresponding crystal structure)

crystallized in a monoclinic cell, as shown in Fig. 1(e).

References

- [1] C. Hecht, F. Stadler, P. J. Schmidt, J. Schmedt auf der Günne, V. Baumann, and W. Schnick, *Chem. Mater.* **21**, 1595 (2009).
- [2] F. Yoshimura, H. Yamane, and M. Nagasako, *J. Solid State Chem.* **258**, 664 (2018).

Keywords: electron microscopy, crystal structure, luminescence

Makoto Nagasako (Corresponding Author, Analytical Research Core for Advanced Materials)

E-mail: nagasako@imr.tohoku.ac.jp

Kazuaki Wagatsuma (Head of Analytical Research Core for Advanced Materials)

E-mail: wagatsuma@imr.tohoku.ac.jp

URL: <http://bunseki-core.imr.tohoku.ac.jp/>

Author Index

Name	page	Name	page
A			
Aoki, Dai	37	Nagai, Yasuyoshi	33, 40, 41
Arima, Hiroshi	19	Nagasako, Makoto	51
B			
Bauer, Gerrit E. W.	26, 47	Nagumo, Kazuaki	33
C			
Chen, Ying	46	Nakamura, Shintaro	49
Chewpraditkul, Weerapong	47	Niinomi, Hiromasa	36
Chiba, Akihiko	11	Nojiri, Hiroyuki	27, 43
E			
Elyasi, Mehrdad	26	O	
F			
Fujita, Masaki	31, 48	Ohta, Hitoshi	43
Fujiwara, Kozo	16	Okamoto, Norihiko L.	20
H			
Hojo, Tomohiko	9	Onose, Yoshinori	32
I			
Ichitsubo, Tetsu	20	Orimo, Shin-ichi	23, 45
Inoue, Koji	33	S	
K			
Kasada, Ryuta	18	Saitoh, Eiji	28
Kato, Hidemi	13, 21	Sakurai, Takahiro	43
Kawaguchi, Tomoya	20	Sasaki, Takahiko	30, 49
Kawazoe, Yoshiyuki	46	Sato, Koji	26
Kikkawa, Takashi	28	Sato, Mitsutaka	8
Kimura, Shojiro	43	Sato, Toyoto	23
Konno, Toyohiko J.	38	Shimizu, Yasuo	33
Kono, Tatsuoki	45	Shiogai, Junichi	29
Kosaka, Wataru	35	Shirasaki, Kenji	50
Kubo, Momoji	17, 46	Suzuki, Tatsuya	40
M			
Masahasi, Naoya	42, 44	T	
Matsuoka, Takashi	34	Takanashi, Koki	22
Matsuta, Hideyuki	12	Tanimura, Hiroshi	20
Miyasaka, Hitoshi	35	Terada, Yayoi	14
Mizukoshi, Yoshiteru	44	W	
Mohri, Tetsuo	14	Wagatsuma, Kazuaki	51
N			
O			
S			
T			
W			
Y			
Z			

Keyword Index

Keyword	page	Keyword	page
A			
actinide	40, 50	high strength steel	9
alloy	11	hydride	23, 45
alpha-ray spectroscopy	50	hydrogen evolution	44, 45
atom probe tomography	33	hydrogen implantation	33
antiferromagnetic	35	I	
antiferromagnets	28	instrumentation	48
C			
computational materials science	14	interface	17
crystal growth	10, 16	L	
crystal structure	20, 23, 51	light yield	47
D			
3D structure	21	(Lu,Gd) ₃ AGG:Ce	47
defects	16	luminescence	51
devices	32	M	
dielectric	38	magnetic properties	12, 22, 42
diffusion	20	magnetism	49
E			
electron microscopy	18, 51	magnetoconductance	30
electronic material	33	mass spectrometry	40
electronic structure	18, 31	mechanical properties	11, 13
energy storage	20, 45	metal	36
epitaxial growth	34	metallic glass	42
F			
fatigue	13	Mg	47
fermi surface	37	microstructure	8, 11, 13
ferromagnetic	35	molecular beam epitaxy (MBE)	29
first principles calculations	46	molecular dynamics	17
foam	21	multi-ferroics	32
fracture	9	N	
frustrated spin system	49	nanostructure	36, 42
G			
GaN	34	neutron scattering	23, 48
GIWAXS	30	nitride semiconductors	34
glow discharge plasma	12, 44	nuclear materials	18, 41
H			
heavy fermion	37	nucleation & growth	36
higher education	14	O	
high magnetic field	27, 43	optical properties	46
high pressure	43	oxide	38
P			
phase transformation			
piezoelectric			
polymer			
porosity			

Keyword	page
Q	
quantum phase transition	43
R	
radiation effects	41
S	
scanning transmission	
electron microscopy (STEM)	41
scintillation decays	47
scintillator	10
short-life alpha-ray emitter	50
simulation	17, 46
solar cells	16
spectroscopy	12
spin current	28
spin excitation	48

Keyword	page
spin wave	26
spintronics	26, 28
steel	8
superconducting	27, 31, 37
synchrotron	19
T	
thin films	22, 29, 38
thermo-electricity	22
topological insulator	29
X	
XAFS	19, 31
X-ray diffraction (XRD)	19
X-ray scattering	27

Editors

Kozo Fujiwara, Ryuta Kasada, Yoshinori Onose,
Shigeyuki Takagi, Takeshi Seki, and Norihiko L.
Okamoto

Editorial Staff

Misa Y. Tomimatsu, Aki Oikawa, and Yuko Godart

Printing

HOKUTO Corporation

Organization

Institute for Materials Research
Tohoku University
2-1-1 Katahira, Aoba-ku, Sendai 980-8577, Japan
Tel. +81-(0)22-215-2144 Fax. +81-(0)22-215-2482

URL: <http://www.imr.tohoku.ac.jp/>
E-mail: pro-adm@imr.tohoku.ac.jp



東北大学 金属材料研究所
Institute for Materials Research
Tohoku University

2-1-1 Katahira, Aoba-ku
Sendai 980-8577, Japan

<http://www.imr.tohoku.ac.jp/>